The Effect of Biological and Polymeric Inhibitors on Methane Gas Hydrate Growth Kinetics

By

Shadi Al-Adel

Department of Chemical Engineering
McGill University
Montreal, Quebec, Canada

May, 2007

A thesis submitted to the Faculty of Graduate Studies and Research in partial fulfillment of the requirements of the Degree of Masters of Engineering

ABSTRACT

Gas hydrates, also known as clathrate hydrates, are non-stoichometric crystalline compounds that have an “ice-like” appearance. They occur when water molecules hydrogen bond to form cavities that can be occupied by a gas or volatile liquid. The inclusion of these guest molecules stabilizes the water network. Hydrates are a nuisance to the gas processing industry as they plug pipelines and equipment which can upset daily operations and add unnecessary maintenance costs.

In this work, kinetic experiments were performed on a methane-water system in the presence of Antifreeze Proteins (AFP`s) in order to elucidate their effectiveness as a kinetic hydrate inhibitor. The results were compared to experiments done with a classical polymeric hydrate inhibitor, N-vinylpryrrolidone-co-N-vinylcaprolactam [poly(VP/VC)] at the same pressure, temperature and weight percent conditions. As well, a series of experiments was conducted on poly(VP/VC) to examine the effect of concentration on hydrate growth inhibition. Experiments were performed at temperatures between 275.15-279.15 K and pressures between 5800-7200 kPa. The effect of the kinetic inhibitors on the hydrate growth profile was examined as well as the effect of temperature and pressure on the performance of the inhibitors.

Two other polymers were tested for hydrate growth for the first time to discover their effect on the kinetics of hydrate formation. The results showed that they promoted the growth of clathrate hydrates.

EXTRAIT

Les hydrates gazeux, aussi connus comme des «clathrates d'hydrate », sont des complexes crystallins non-stœchiométriques ayant l'apparence de la glace, mais composés d'une structure différente. Ils se forment quand des molécules d'eau se lient grâce aux liens hydrogène pour former des cavités qui peuvent être occupés par un gaz ou un liquide volatil. L'introduction de ces molécules «invités» stabilise la structure formée par les molécules d'eau. Les hydrates sont une nuisance pour l'industrie de développement de gaz parce qu'ils peuvent obstruer les pipelines et équipements, ce qui interromperait les opérations quotidiennes et ajouterait aux coûts de maintenance.

Dans cette étude, des expériences cinétiques ont été effectuées sur des systèmes méthane-eau en présence de protéines antigel (AFP's) pour déterminer leur efficacité comme inhibiteurs cinétiques d'hydrates. Les résultats ont été comparés aux résultats obtenus avec des polymères inhibiteurs d'hydrates classiques, N-vinylpryrrolidone-co-N-vinylcaprolactam [poly(VP/VC)], avec la même pression, température et pourcentage de masse en inhibiteur. De plus, une série d'expériences a été conduite avec le poly (VP/VC) afin d'examiner l'effet de la concentration du polymère sur l'inhibition de la croissance d'hydrates. Les températures et pressions examinées variaient respectivement de 275.15 à 279.15K et de 5800 à 7200 kPa. L'effet des inhibiteurs cinétiques sur le profil de la croissance d'hydrates a été examiné ainsi que l'effet de la température et de la pression sur la performance des inhibiteurs.

Deux autres polymères ont été testés pour la première fois pour étudier la croissance d'hydrates et découvrir leurs effets sur la cinétique de formation des hydrates

gazeux. Les résultats obtenus ont démontré que ces polymères favorisent la croissance d'hydrates.

ACKNOWLEDGMENTS

I would like to thank Dr. Phillip Servio for his supervision and support during the past two years. He inspired me to enjoy research and always seek more answers. I would also like to thank Dr. Milan Maric for his support related to information on polymers. He always had answers for the questions I had regarding polymers and was the one to recommend the new polymers that I tested. I thank my lab group for their assistance and support; John for teaching me how to use the lab apparatus and analyze the data and results. Jason and André for their support with the course material, assistance with the apparatus and the useful discussions we had when I was conducting my experiments and analyzing the data. Sebastien for his skill with Matlab and Juan for his advice and discussions. I would also like to thank; Hall, Yeshai, Rasha, Naomi, and Lindsay.

I would like to thank Natural Sciences and Engineering Research Council of Canada for financial sponsorship, as well as the Canada Research Chair program and the Canadian Foundation for Innovation. Last but not the least, I would like to thank Saudi Aramco for sponsoring my Master's program and specifically Yuv Mehra who is my mentor for his continuous support and follow up on my progress.

TABLE OF CONTENTS

LIST OF FIGURES

LIST OF TABLES

1 INTRODUCTION

1.1 Background

Gas hydrates also known as Clathrate hydrates are nonstoichiometric, crystalline compounds, which consist of a host lattice of molecules of water that encages a guest molecule. The water lattice is held together through hydrogen bonding but is not thermodynamically stable without the presence of the guest molecule which interacts with the host lattice through weak Van Der Waals forces. There is no chemical reaction between the host and guest molecules (Bishnoi and Natarajan, 1996).

The discovery of gas hydrates in laboratories came as early as 1810 when Sir Humphry Davy found that an aqueous solution of chlorine formed a crystalline solid when cooled to 9ºC. Thirteen years later, John Faraday confirmed these results and until the 1930s, research conducted on gas hydrates was purely academic. The industry became interested in gas hydrates in 1934 soon after Hammerschmidt discovered that hydrates can form in gas and oil pipelines and cause major operation upsets by clogging pipelines and major equipment such as heat exchangers (Englezos, 1993). As a result of this major discovery, a great deal of research took place in order to understand hydrate formation and develop several different ways to inhibit their formation. In the 1960s research in gas hydrates took another major step forward after the discovery of vast quantities of natural gas hydrates in the earth's crust (Englezos, 1993). The amount of natural gas reserves found within hydrates is estimated to be 2×10^{16} m^3, which is believed to be almost twice as much as the fossil fuel reserves (Whiticar, 2001). These discoveries lead scientists to focus their efforts on finding safe and economical methods for recovering the natural gas from gas hydrates.

Gas hydrates are also being considered as means for gas storage and transportation natural gas can be trapped in the cages of the gas hydrate (Englezos 1993). In terms of storage, hydrates have a unique positive property where they can contain 180 + volumes of natural gas per volume of hydrate at standard temperature and pressure (STP). Storing in hydrate form is also appealing with regards to safety concerns. In case of storage tank ruptures the release of natural gas from hydrates is slow. Another safety advantage is the fact that flammable gases are encased in ice and finally hydrates can be stored under relatively low pressures compared to other transportation methods such as Liquefied Natural Gas (LNG) (Zhong and Rogers, 2000). Natural gas hydrates could be considered as a threat to the environment. There are concerns that global warming in the earth might be able to raise the temperature above the equilibrium hydrate temperature. This can cause hydrate decomposition where a massive quantity of natural gas would be released to the atmosphere. Natural gas hydrates can actually contribute more negatively on global warming than carbon dioxide since methane has a global warming potential 21 times larger than that of carbon dioxide (Englezos, 1993).

Although a lot of research has been done with regards to inhibition and several inhibitors are used widely in the industry such as methanol and glycols, they are not environmentally friendly and are used in high quantities and concentrations. A challenge still exits to find an effective inhibitor which is environmentally acceptable and used in small concentrations and quantities in order to minimize pollution, reduce cost, decrease product contamination and increase pipeline production.

1.2 Hydrate Formation and Structure

The hydrate structure consists of a host, which forms the lattice and a guest component, which fills the cage within the lattice. Without the presence of the guest molecule, the host lattice is thermodynamically unstable. It is important for the guest molecule to be within a specific size range in order to fit into the cage of the host lattice. Very large guest molecules will interfere with the hydrogen bonding of the water lattice while very small molecules will be unable to stabilize the host cage. Generally, guest molecules with a diameter smaller than 3 Å can not form a stable hydrate crystal. Examples are helium, hydrogen and neon (Sloan, 1998). There are three naturally occurring gas hydrates structures known to exist and they are: structure I, structure II and structure H (Sloan 1998). They are made of basic crystal cavities that differ in their configuration.

As seen in Figure 1.2.1, Structure I hydrates form two types of cavities. The first one forms a structure with 12 faces and 5 sides, which is known as a pentagonal dodecahedron (5^{12}). The second cavity is larger and has 12 pentagonal faces and 2 hexagonal faces, known as a tetrakaidecahedron ($5^{12}6^2$). Molecules with a diameter between 4.2-6.0 Å can form structure I hydrates (Sloan, 1998). Common guest molecules that form structure I hydrates are methane, ethane and carbon dioxide.

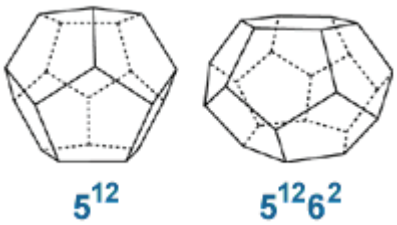

Figure 1.2.1 - Cages of Structure I Hydrate (adapted from www.pet.hw.ac.uk)

Unlike structure I hydrates that are formed by the vertices, structure II hydrates are formed when the pentagonal dodecahedrone links together through face sharing. This structure consists of two faces as seen in Figure 1.2.2, which are a small cage of hexakaidecahedron (5^{12}) and a larger polyhedron cage with 12 pentagonal and 4 hexagonal (5^{12} 6^4). Structure II hydrates are made up 136 water molecules and consist of 16 small and 8 large cavities. This structure of hydrates can only be formed by molecules with a diameter of 6-7 Å. Propane and iso-butane can form this type of hydrate structure (Sloan, 1998).

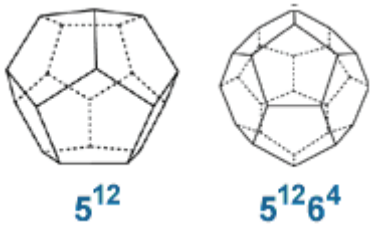

Figure 1.2.2 - Cages of Structure II Hydrate
(adapted from www.pet.hw.ac.uk)

Larger molecules, which are too large to stabilize structure I & II form structure H hydrates. This structure was discovered in 1987 by Ripmeester (Ripmeester et. al, 1987). Structure H hydrates comprises of three different types of crystal cavities, where two are small and the third is large and non-spherical. The first type is the basic 5^{12} that is found in structures I and II. The two other types are the 12 face $4^3 5^6 6^3$ and large $5^{12}6^8$ cavities (see Figure 1.2.3). The $4^3 5^6 6^3$ cavity has three square faces, six pentagonal faces, and three hexagonal faces, whereas the $5^{12}6^8$ cavity has 12 pentagonal faces and eight hexagonal faces. Structure H hydrates consists of 34 water molecules (Ripmeester et. al, 1987). Unlike structure I & II, structure H hydrates require molecules of two different sizes to stabilize the crystal. Large molecules with a diameter up to 9 Å can fit inside the cavity of this hydrate structure. Examples of guest molecules that can form this structure

are neohexane, admantane and cycloalkanes such as cycloheptane (Ripmeester et. al, 1987).

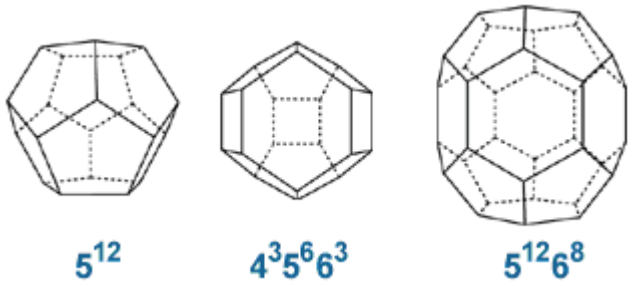

Figure 1.2.3 -Cages of Structure H Hydrate (adapted from www.pet.ac.uk)

1.3 Phase Equilibrium

It is necessary to know the equilibrium hydrate-forming conditions for the rational and economic design and operation of processes in the oil and gas industries where hydrates are encountered. Gas hydrate phase equilibrium research focuses on finding the incipient formation conditions of hydrates at specified pressure and temperature conditions (Englezos, 1993). For gas and oil facilities, it is important to know the operating condition at which hydrates can form in order to operate far away from the hydrate equilibrium conditions and maintain smooth and safe operation. The following phases might be present at incipient equilibrium in a hydrate forming system: solid hydrate, aqueous liquid, non-aqueous liquid, gas and ice.

Laboratory experiments are conducted in order to create phase equilibrium plots for different guest and host molecules by the use of the so-called isothermal pressure search method (Englezos, 1993). In this method hydrates are formed at a constant temperature and various pressures. At a certain temperature the pressure of the system is increased in order to form hydrates. The pressure is then slowly released at a constant temperature until a small amount of hydrate is present. This is the equilibrium pressure

and any further decrease of pressure would cause the crystal phase to disappear (Englezos, 1993). This procedure is then repeated at various temperatures in order to produce a temperature-pressure equilibrium curve. Different equilibrium curves are produced depending on the host and guest molecules in the system. An example of a partial phase diagram for the methane/water system is given below in Figure 1.3.1.

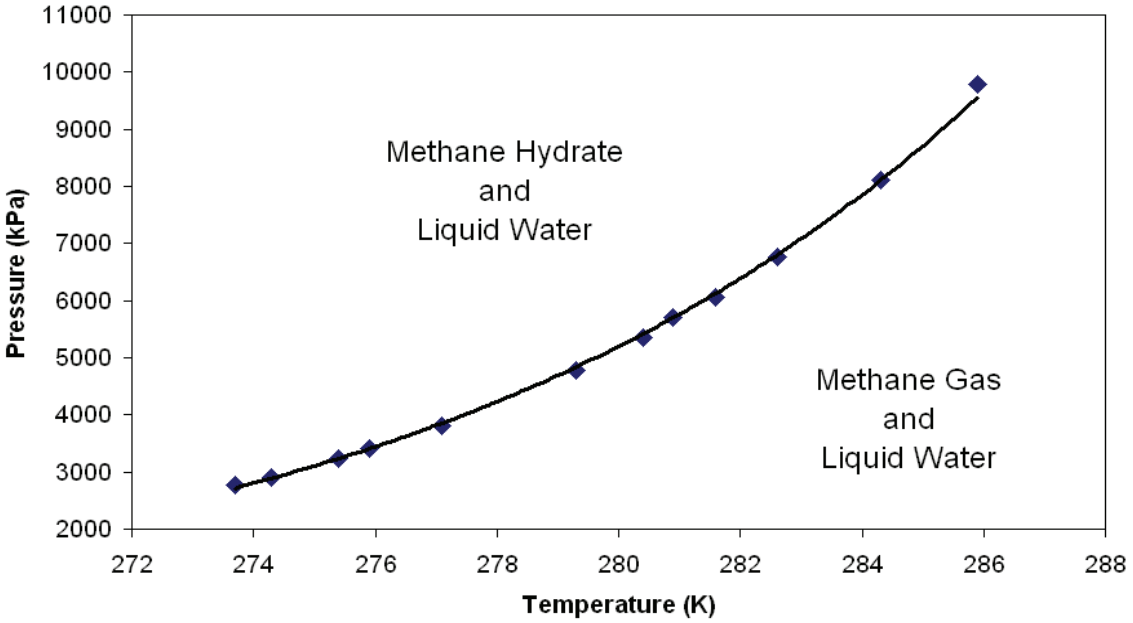

Figure 1.3.1 - Three Phase Equilibrium Curve for a Methane-Water System (adapted from Deaton and Frost, 1946)

1.4 Kinetics of Hydrate Formation and Decomposition

There are two fundamental steps involved with the hydrate kinetic formation. The first one is the time period required for a hydrate to reach a critical size nucleus and the second is the hydrate growth rate after the critical size nucleus has been achieved (Bishnoi and Natarajan, 1996). Figure 1.4.1, illustrates the two steps of hydrate kinetic formation, which are the nucleation and growth period.

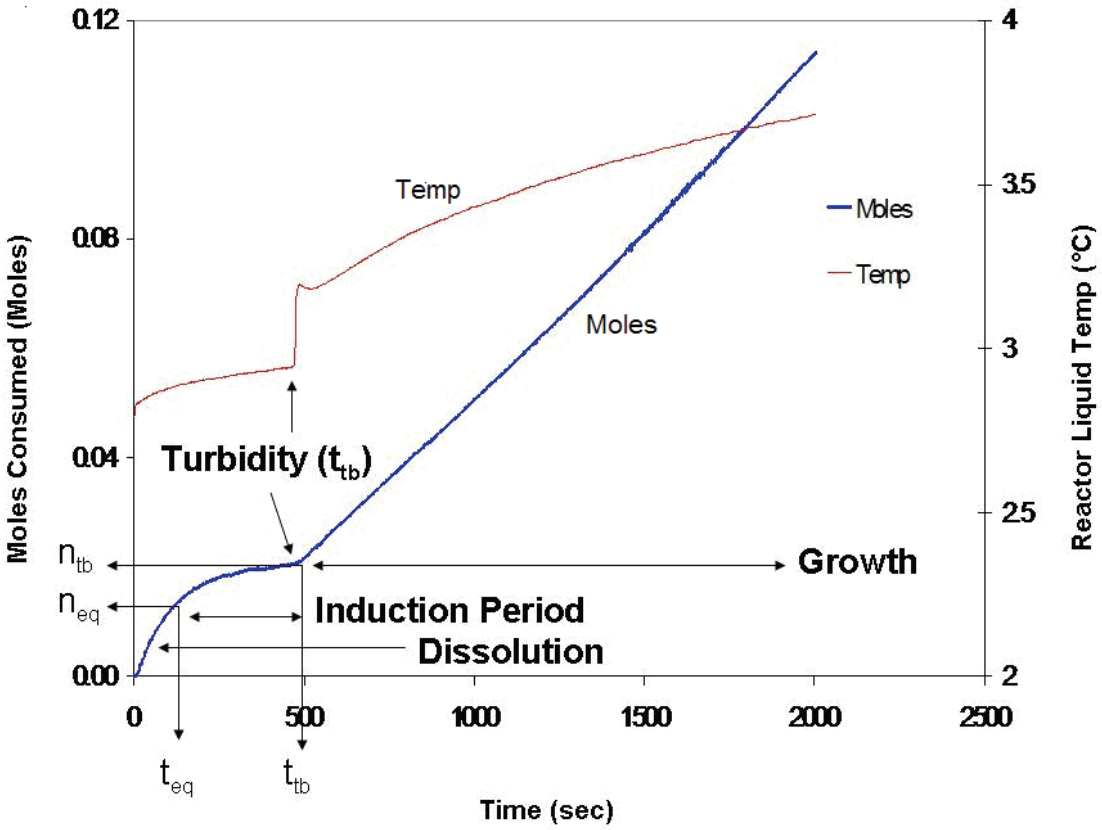

Figure 1.4.1 - Typical Gas Mole Consumption Plot

Initially the gas dissolves in water until the water becomes supersaturated with gas. Then hydrate nucleation occurs when small hydrate crystals called nuclei grow and disperse until a critical size for continued growth is achieved. Once this stable nucleus is formed, the hydrate lattice will grow by adsorbing gas molecules from the surrounding liquid, which is known as the growth period.

Induction time is the period a hydrate crystal take to reach a critical size and then become stable. As seen in Figure 1.4.1, the induction period starts at t_{eq} and ends at the turbidity point (t_{tb}). The turbidity point is the point where the induction period ends and the first appearance of stable hydrate crystals occurs, which also denotes the beginning of the hydrate growth. The amount of moles consumed at t_{eq} is represented by n_{eq} and n_{tb} is

defined as the total number of moles consumed up to the turbidity time. The amount of gas consumed during the formation of the hydrate nuclei can be calculated by calculating the difference between n_{tb} and n_{eq} (Servio, 2002). It can also be noticed from Figure 1.4.1 that at the turbidity point, there is a spike in the temperature, which is a result of hydrate formation being an exothermic process. After the hydrate nuclei achieve the critical size they start the process of growth where hydrate crystals form. As shown in Figure 1.4.1, the growth starts at the turbidity point.

1.4.1 Hydrate Nucleation

Hydrate nucleation also called the induction period is the process where small hydrate crystals nuclei grow and disperse until they reach a critical size or radius for continuous growth (Bishnoi and Natarajan, 1996). Two types of nucleation exist; homogeneous and heterogeneous. Homogenous nucleation is a solidification process that occurs in systems with no impurities. In reality nucleation is nearly always heterogeneous since it is almost impossible not to have foreign particles present. The presence of foreign particles reduces the amount of energy required to form a stable nucleus (Bishnoi and Natarajan, 1996).

After extensive studies performed on the nucleation of gas hydrates, which did not result in predicting it, nucleation is considered to be a stochastic process. Although the nucleation period is considered stochastic, researchers managed to determine certain factors that affect it, which are shown below:

1. History of water (Natarjan et. al, 1994).
2. Degree of supersaturation (Bishnoi and Natarajan, 1996).
3. Stirring rate (Englezos et. al, 1987).

4. Temperature and pressure (Sloan, 1990).
5. Molecular diameter to cavity size ratio (Sloan, 1990).

Experiments conducted by Vysniaukas and Bishnoi revealed that there was a history effect of water on the induction time (Vysniaukas and Bishnoi, 1983). They also concluded that water obtained from dissociated hydrates had shorter induction periods than water used from hot tap water (Bishnoi and Natarajan, 1996). The concentration of the dissolved gas in the solution divided by the amount of dissolved gas corresponding to the three phase equilibria is defined as supersaturation. Natarajan and co-workers discovered that the induction time increases with a decrease in the supersaturation (Natarjan et. al, 1994). It was found that that the stirring rate affects the induction period as higher stirring rates resulted in faster induction times (Englezos et. al, 1987). Temperature and pressure also affect the induction period as low temperatures and high pressures result in short induction periods (Sloan, 1990). Sloan proved that the hydrate structure stability is affected by the size of the guest molecules as some molecules were better in stabilizing the hydrate. It was then concluded by him that the higher the stability of the guest molecule the shorter the induction periods are (Sloan, 1990).

1.4.2 Hydrate Growth

Hydrate growth refers to the growth of stable hydrate nuclei as solid crystals after they reach the critical size (Bishnoi and Natarajan, 1996). The same factors that affect nucleation, which were mentioned in the previous section along with heat and mass transfer also affect the growth (Englezos et. al, 1987). Unlike nucleation, models have been developed for growth.

1.4.2.1 Background of Hydrate Growth Kinetic Models

Vysniaukas and Bishnoi mentioned that their kinetic experiment results on methane indicated that hydrate formation kinetics is a function of interfacial area, temperature, pressure and degree of supercooling (Vysniaukas and Bishnoi, 1983). They considered that rate of hydrate formation is a function of the concentrations of critical cluster and the water/methane monomers at the interface and the total surface area of the gas-water interface. The approach they used with regards to hydrate formation was a hydrate reaction approach that had the temperature difference as a driving force. The rate of hydrate formation was described as follows:

$$r \approx k_r a_s D^n [H_2O]^{m+n} [M]^{q+n} \exp\left(\frac{-a'}{\Delta T^b}\right) \qquad \textbf{Eqn 1.4.1}$$

where k_r is a lumped Arrhenius type reaction rate constant. a_s is the totalled surface area of the gas-water interface. D is an arbitrary constant and a' and b are two empirical constants. The terms contained within the parentheses are the concentrations of the three components. The methane rate of consumption during hydrate formation is represented by m, n and q, which are parameters that indicate the order of reaction with respect to each component. ΔT^b represents the supercooling given by the difference the hydrate forming equilibrium temperature at any pressure and the experimental temperature (Vysniaukas and Bishnoi, 1983).

In 1987 Englezos et al. developed a model for methane and ethane hydrates, which described the hydrate growth rate (Englezos et al., 1987). He proposed that the overall driving force for crystallization is given by the difference in the fugacity of the dissolved gas and the three-phase equilibrium fugacity at the experimental temperature, which can be represented by the following:

$$\Delta f = f - f_{eq} \qquad \textbf{Eqn 1.4.2}$$

It should be noted that the driving force is determined by the deviation from equilibrium rather than the magnitude of the experimental pressure.

Two steps for growth were proposed (Englezos et al., 1987) to explain the model, which are :

1: Diffusion of the dissolved gas from the bulk of the solution to the crystal-liquid interface through the laminar diffusion layer around a particle.

2: "Reaction" at the interface, which is an adsorption process that describes the incorporation of the gas molecules into water molecules and subsequent stabilization of the framework of the structured water.

Since no accumulation is permitted in the diffusion layer around the particle, the rates of the two above steps are equal. As a result, the growth rate per particle in terms of the overall driving force can be obtained by the following equation (Englezos et al., 1987):

$$\left(\frac{dn}{dt}\right)_P = K^* A_P \left(f - f_{eq}\right) \qquad \textbf{Eqn 1.4.3}$$

Where A_P is the surface area of each hydrate particle and the value of the global rate K^* is given by:

$$\frac{1}{K^*} = \frac{1}{k_d} + \frac{1}{k_r} \qquad \textbf{Eqn 1.4.4}$$

Where k_d is the mass-transfer coefficient around the particles and k_r is the reaction rate constant. It should be noted that the outside surface of the surrounding is equal to the inside one, which is the surface of the particle. Regarding the geometry, the hydrate particle shape is assumed to be spherical (Englezos et al., 1987). Eg. 1.4.3 described the

gas consumed per particle. To describe what occurs to the gas phase when it contacts a liquid phase, the two-film theory was used. A quasi-steady state was assumed as the accumulation term in the liquid film is neglected. This results the mass balance for the gas in the film in a slice of thickness d*y* to yield the following equation (Englezos et al, 1987):

$$D\frac{d^2c}{dy^2} = K\left(f - f_{eq}\right) \qquad \textbf{Eqn 1.4.5}$$

Where *D* is the diffusivity of the gas, *c* the concentration of the gas, *y* the distance from the gas-liquid interface and $K = 4\Pi K^{*}\mu_2$, where μ_2 is the second moment of the particle size distribution. It is given by the following:

$$\mu_2 = \int_0^{\infty} r^2 \phi(r,t)dr \qquad \textbf{Eqn 1.4.6}$$

Where $\phi(r,t)$ us the crystal six distribution, *r* the particle radius and *t* is the time (Englezos et al, 1987).

Skovborg and Rasmussen developed a simplified model of the Englezos model, which based the gas consumption on the rate of mass transfer. Their model was based on the following (Skovborg and Rasmussen 1994):

1. Equilibrium in the water bulk phase exists between the liquid water and the hydrate particles along with the dissolved gas.
2. The liquid phase and gas phase are in equilibrium at the interface.
3. According to a simple film theory, the gas is transported from the gas-liquid interface to the bulk water liquid phase.

The gas consumption the rate of mass transfer was then defined as:

$$\frac{dn}{dt} = k_L A_{(s-l)} c_{w0} \left(x_{\text{int}} - x_b \right)$$ **Eqn 1.4.7**

Where $A_{(s-l)}$ is the gas-liquid interfacial area and c_{w0} is the initial concentration of water. x_{int} is the mole fraction of gas in the water phase at the water-gas interface in equilibrium with the gas phase at the experimental pressure and temperature. x_b is the moles fraction of the gas in the bulk water phase in equilibrium with the hydrate phase at the experimental pressure and temperature. k_l is mass transfer coefficient and defined as follows: $k_L = \frac{D}{y_L}$ **Eqn 1.4.8**

Where D is the diffusivity and y_L is the film thickness (Skovborg and Rasmussen 1994).

1.4.2.2 Determining the Global Reaction Constant Using a New Growth Model

A new comprehensive model for the growth has been derived from the model that Englezos et. al developed in 1987 (Englezos et. al, 1987). The model defines the change in the mole consumption rate during growth at constant pressure as follows (Bergeron and Servio, 2007):

$$\left(\frac{dn}{dt}\right)_p = \frac{V_L \rho_w}{MW_w} K^* (x^i_{G-L} - x^i_{H-L})$$ **Eqn 1.4.9**

Where V_L is the volume of solution, ρ_w and MW_w are the density and molecular weight of water respectively, x^i_{G-L} *and* x^i_{H-L} are the mole fraction in the gas liquid and hydrate liquid phases respectively. Finally K^* is the global reaction rate constant, which comprises of the resistances that the gas molecule faces during hydrate formation. Those

resistances will be explained using the schematic shown in Figure 1.4.2, which explains these resistances in a three-phase equilibrium system.

Initially, the gas molecule dissolves into the liquid and the first resistance it faces is the resistance to reach the gas-liquid interface ($\frac{1}{K_g A_i}$), which is a small resistance. K_g is the diffusion rate constant into the gas film and A_i is the area of the gas-liquid interface. Then the gas molecule faces a larger resistance ($\frac{1}{K_l A_i}$), which is the resistance the gas molecular faces when it starts penetrating into the bulk liquid. This resistance can be eliminated with sufficient stirring and mixing. K_l is the diffusion rate constant into the liquid. The mole fraction remains constant in the bulk liquid phase as long as there is sufficient mixing. When the gas molecule starts entering the hydrate phase, it faces another small resistance at the hydrate surface ($\frac{1}{K_d A_p}$), where K_d is the diffusion rate constant in the hydrate film and A_p is the surface area of the hydrate particle. Then, the fourth and final resistance is the resistance that the gas molecule faces when it reacts and forms the hydrate particle ($\frac{1}{K_r A_p}$), where K_r is the intrinsic reaction rate constant in the hydrate film. This resistance is a much larger than the resistance at the hydrate film.

By summing up all the four resistances, K^* can be expressed as the following (Bergeron and Servio, 2007):

$$K^* = \frac{1}{\frac{1}{K_l A_i} + \frac{1}{K_r A_p} + \frac{1}{K_d A_p} + \frac{1}{K_g A_i}} \qquad \textbf{Eqn 1.4.10}$$

Since the resistances due to the diffusion in the gas-liquid and hydrate-liquid interfaces are small compared to the other two, they can be neglected; hence K^* is reduced to the following expression:

$$K^* = \frac{1}{\frac{1}{K_l A_i} + \frac{1}{K_r A_p}} \qquad \textbf{Eqn 1.4.11}$$

By substituting this expression for K^* in equation 1.4.9, the rate of mole consumption becomes the following:

$$\left(\frac{dn}{dt}\right)_p = \frac{V_L \rho_w}{MW_w} \frac{(x^i_{G-L} - x^i_{H-L})}{\frac{1}{K_l A_i} + \frac{1}{K_r A_p}} \qquad \textbf{Eqn 1.4.12}$$

This equation (Bergeron and Servio, 2007) describes the global reaction rate constant for a methane and ethane system and represents the new model for hydrate growth.

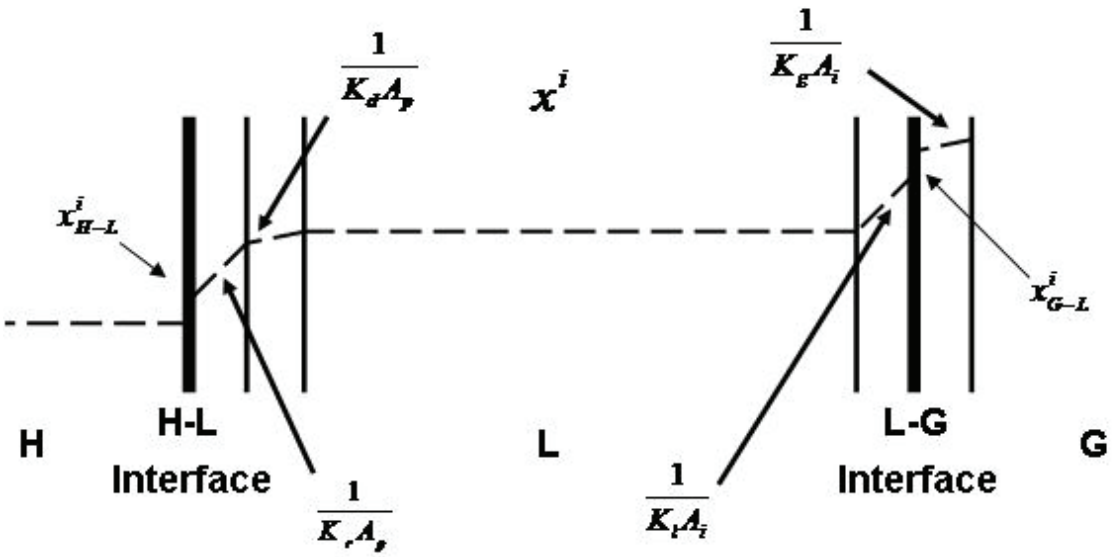

Figure 1.4.2 – Solubility of a gas molecule in a three phase equilibrium system

1.4.3 Hydrate Decomposition

Unlike hydrate growth, decomposition has not been studied extensively, but fortunately it has similar properties to growth (Bishnoi and Natarajan, 1996). The decomposition process is considered as an endothermic process that produces water and the gas that was engaged within the hydrate lattice. Hydrate decomposition consists of two consecutive steps that occur at the solid surface (Bishnoi and Natarajan, 1996):

1. Destruction of the hydrate host lattice at the surface of the particle.
2. Desorption of the guest molecule from the surface into the reaction layer, and then the gas diffuses from the reaction layer into the bulk (Servio, 1998).

In 1986, Kim et al, developed a kinetic model for hydrate decomposition. Assuming the hydrate particles were spherical, he considered that they were surrounded by a cloud of gas (Bishnoi and Natarajan, 1996). Kim also assumed that the rate of hydrate decomposition $-\left(\frac{dn_H}{dt}\right)$, was proportional to the combined surface area of the decomposing particles, A_s and the driving force. The driving force was proposed to be the difference between the fugacity of the gas at the three phase equilibrium pressure, f_{eq} and the fugacity of the gas at the solid surface. The fugacity of the gas at the solid surface and at the bulk phase, f_g were assumed the same. The heat and mass transfer effects were eliminated since the decomposition data were taken at a high stirring rate (Bishnoi and Natarajan, 1996).

$$-\left(\frac{dn_H}{dt}\right)_P = K_d A_P \left(f_{eq} - f_g^V\right) \qquad \textbf{Eqn 1.4.13}$$

Where K_d is the decomposition rate constant and A_p is the particle surface area. The decomposition driving force is defined by the fugacity difference $\left(f_{eq} - f_g^V\right)$ (Bishnoi and Natarajan, 1996).

1.5 Hydrate Inhibition

Ever since the discovery of hydrates in gas pipelines, the energy industry has considered gas hydrates as a serious problem and gave it major importance. The problem with hydrates rises because their formation can lead to plugging of pipelines and major equipment such as heat exchangers, compressors and pumps. Such plugs in equipment may trip or damage it, which also results in major operation upsets and downtime. Plugs in pipelines cut the production or transportation of fluids, which leads to major cost issues. A lot of effort, research and money have been spent in order to inhibit their formation and prevent them from plugging pipelines and equipment. On an annual basis, it is believed that $500,000,000 is spent on hydrate inhibitors; mostly methanol (Lederhos et. al, 1996).

In industry gas hydrates are common to form in production facilities that encounter low ambient temperatures especially in deep offshore wells. They can also form in the inlet area of processing plants downstream three-phase separates where the water saturated gas's temperature is reduced as a result of the gas expansion caused by the separator. Hydrates can also be formed in other processes that chill down water saturated gas to low temperatures using heat exchangers. When hydrate plugs are encountered in a gas or oil facility and result in a shutdown or production flow discontinuation, a lot of time and effort is spent to remove them. Hydrate inhibitor chemicals such as methanol are used widely to decompose the hydrates and restore fluid

pipeline flow. After extensive research was done to find effective inhibitors, several methods for hydrate inhibition have been developed but the challenge remains on determining the most suitable and cost effective one. Hydrate inhibition can be classified into two categories: thermodynamic and kinetic.

Thermodynamic inhibition is achieved by operating at conditions, which do not form hydrates where the operating temperature and pressure are outside the region that stabilizes the formation of hydrates (Sloan, 1998). Kinetic inhibition does not prevent the hydrates from forming; however it prevents the growth and agglomeration of hydrate crystals. It can be used in the industry to prevent plugging of pipelines and equipment where hydrates that are formed would be carried through the fluid as fine particles, which does not cause plugging (Sloan, 1998).

1.5.1 Thermodynamic Inhibition

Thermodynamic inhibition can be achieved using four methods: temperature increase, pressure decease, removal of the hydrate forming components (gas or water), and finally injection of chemical hydrate inhibitors.

1.5.1.1 Temperature Increase

This method is achieved by operating the process at temperatures above the hydrate equilibrium temperature. This can be done by the use of heat exchangers that heat the fluid or partial isolation of exchangers that cool the fluid. In some circumstances this method can be uneconomical depending on the size of the required equipment to increase the temperature or the size of the pipeline that requires the heating (Sloan, 1998).

1.5.1.2 Pressure Decrease

Pressure reduction can be effective to prevent hydrate formation during pipeline shutdowns; however it is unpractical during normal operation (Sloan, 1998). For certain processes such as cryogenic hydrocarbon recovery, pressure reduction upstream the process is not favorable as it would decrease the hydrocarbon recovery rates.

1.5.1.3 Removal of Host/Guest Molecule

It is more practical to remove the host molecule, which is water since without it hydrate formation would not be possible. Water removal or dehydration is usually done prior to the process where the water dew point of the process gas is lowered below the operating temperature to prevent liquid water from forming, which eventually prevents hydrate formation. Glycols are well known for water removal. The most common glycol used in the gas processing industry for dehydration is triethylene glycol (TEG). For processes that operate at very low temperatures, which are lower than -40°C glycols are not efficient and the use of other chemicals is necessary. Solid desiccants or zeolites such as silica gel, activated alumina and molecular sieves are used to achieve very low water dew points. The use of molecular sieves is most common in the gas processing industry to produce water dew points below -100°C. It is worth mentioning that most dehydration processes have high capital and operating cost, especially molecular sieve dehydration systems.

1.5.1.4 Chemical Hydrate Inhibitor Injection

Chemical inhibitor injection is a very common method of hydrate inhibition. Rather than removing the water to prevent hydrate formation. Inhibitors prevent the water from structuring the way it needs to form hydrates; therefore it increases the required

pressure at a certain temperature to form a hydrate. The most common inhibitors are methanol and glycols such as ethylene glycol (EG) (Sloan, 1998).

Methanol increases the hydrate formation pressure by bonding with water molecules in a certain way where water molecules can not structure themselves into hydrate lattice. Furthermore, the methyl group in methanol competes with the guest molecule for the position in the cavity of the hydrate and prevents it from becoming stable (Sloan, 1998). Glycols inhibit hydrate formation in the same way methanol does; however they are less effective because the glycol molecules are larger in size than methanol. In general, the larger the size of the inhibitor is, the weaker it is with regards to hydrate inhibition (Sloan 1998). At cryogenic temperatures (lower than -40°C), methanol injection becomes more effective because glycols become too viscous and their recovery by separation becomes challenging. Common glycols are ethylene glycol (EG), diethylene glycol (DEG) and triethylene glycol (TEG). The most common one however is EG because of its lower viscosity, lower cost and lower solubility in liquid hydrocarbons (GPSA, 1998). Electrolytes such as sodium chloride, potassium chloride and calcium chloride are also known to be hydrate inhibitors. Electrolytes contact water and get divided into positive and negative ions where every ion bond with several water molecules by dipole-bonds. This prevents water molecules from forming hydrate lattices (Sloan, 1998). Finally polymers such as polyethylene oxide can be considered as thermodynamic inhibitors; however they are weaker than other inhibitors that include electrolytes, methanol and glycols.

Thermodynamic inhibition might not be practical in some scenarios where they could be costly in offshore or remote production facilities. One of their major drawbacks

is the fact that they are used in high concentrations (10-50 wt%) (Mizuta, 2006). The more the temperature and pressure conditions become sever, the higher the required concentration becomes. At some extreme cases, the required concentration might increase dramatically up to 60 wt% (Koh et. al, 2002). An example can be given with regards to a processing plant that operates with a gas flow of 5.66×10^6/day and a water content of 3.16×10^4 kg/day. A typical required methanol quantity per water removed is 0.65 kg for each kg of water. Based on this required quantity, the amount of methanol to be used will be 2.4×10^4 L/day. With an estimated methanol cost of $0.56/L, the cost due to methanol use is around $ 5 million per year, which is considered as a significant amount for such a small facility (Koh et. al, 2002).

1.5.2 Kinetic Inhibition

Kinetic inhibition, also called low dosage hydrate inhibitors (LDHI) since the inhibitors are used in low concentrations, was introduced in the last 10-15 years (Kelland et. al, 2006). Unlike thermodynamic inhibitors that require 10-50 wt%, most LDHI need only 0.1-1 wt% concentrations (Kelland et. al, 2006). There are two different types of kinetic inhibition; anti-agglomerants and kinetic inhibitors. Anti-agglomerants prevent hydrates from agglomerating through emulsifying the water into a liquid hydrocarbon phase, while kinetic inhibitors prevent the hydrate from growing above the critical size (Kelland et. al, 2006).

1.5.2.1 Anti-Agglomerants

Anti-agglomerants (AA) prevent hydrate particles from agglomerating to larger masses. They stabilize the internals of the water phase to a liquid hydrocarbon phase as an emulsion rather than to a hydrate crystal. Surfactants are the most effective chemicals

that act as anti-agglomerants as they provide a relatively stable water-oil emulsion (Sloan, 1998). In comparison to the traditional thermodynamic inhibitors, only small amounts of surfactant injection are required. Behar suggested in 1994 that 1 wt% of surfactant is equivalent to 25 wt% of methanol (Sloan, 1998).

1.5.2.2 Kinetic Inhibitors

The function of kinetic inhibitors is to delay hydrate nucleation and slow down hydrate crystal growth. The hydrate crystal growth slows down significantly when kinetic inhibitors are used. Kinetic inhibitors sustain the hydrate's small size by absorbing onto the hydrate crystal surface in order to block the crystal growth (Lederhos et. al, 1996).

Polyvinylpyrrolidone also known as PVP was found to be the first promising kinetic inhibitor. Defined as a first generation inhibitor (Lederhos et. al, 1996), PVP consists of five-member lactam rings attached to a carbon backbone. Lactam rings are characterized by an amide group, (-N-C=O), which is attached to the polymer backbone (Lederhos et. al, 1996). There are three other classical kinetic inhibitors (see Figure 1.5.1), which are considered as second generation inhibitors were discovered. They belong to the same lactam ring polymer family as PVP. The names of the three inhibitors are: (Lederhos et. al, 1996):

1. Poly (N-vinylcaprolactam) or PVCAP.
2. A terpolymer of N-vinylpyrrolidone /N-vinylcaprolactam/N, Ndimethylaminoethylmethacrylate or VC-713.
3. A copolymer of N-vinylpryrrolidone-co-N-vinylcaprolactam, which is also known as poly(VP/VC).

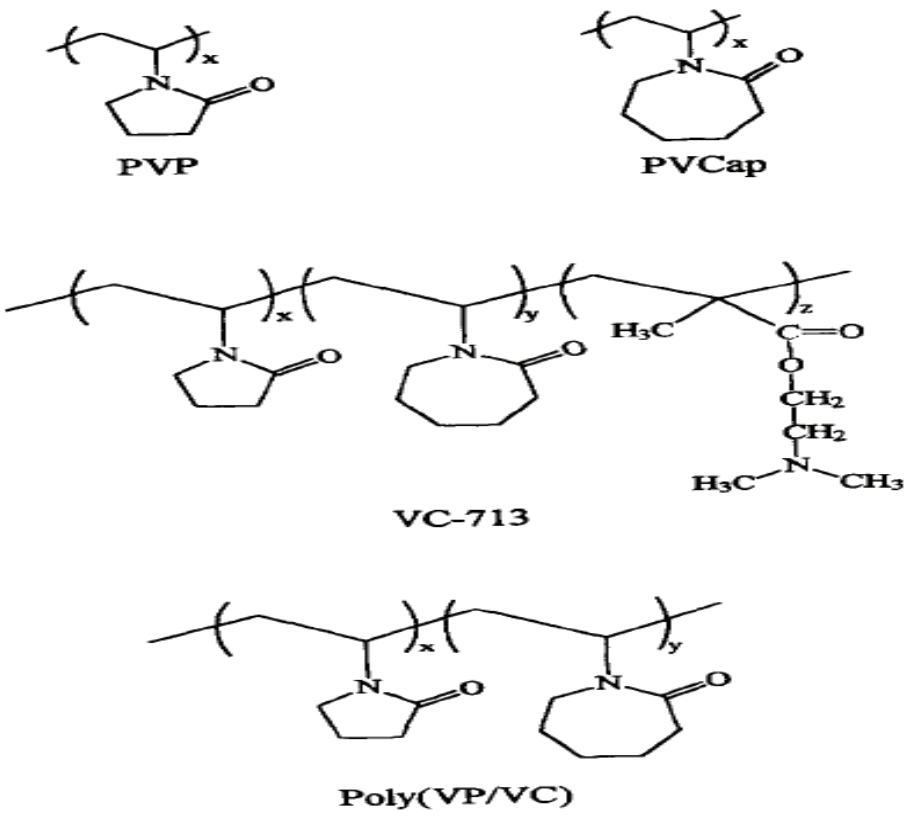

Figure 1.5.1 - The chemical structure of different polymer kinetic inhibitors (adapted from Lederhos et. al, 1996)

All of the three kinetic inhibitors listed above were tested by Lederhos et. al and found to be much more effective than PVP, especially at lower temperatures. At relatively low temperatures PVP was found to be ineffective in terms of hydrate inhibition. It was found that at temperatures down to 277 K, PVP promoted the formation of hydrates instead of inhibiting their formation (Lederhos et. al, 1996). Several studies have showed PVCAP to be a better inhibitor than PVP although the main difference between the two polymers is that PVCAP contains two carbons more than the PVP ring (Kvamme et. al, 2005). As seen from Figure 1.5.2, the mole consumption of PVCAP is a lot lower than the mole consumption of PVP.

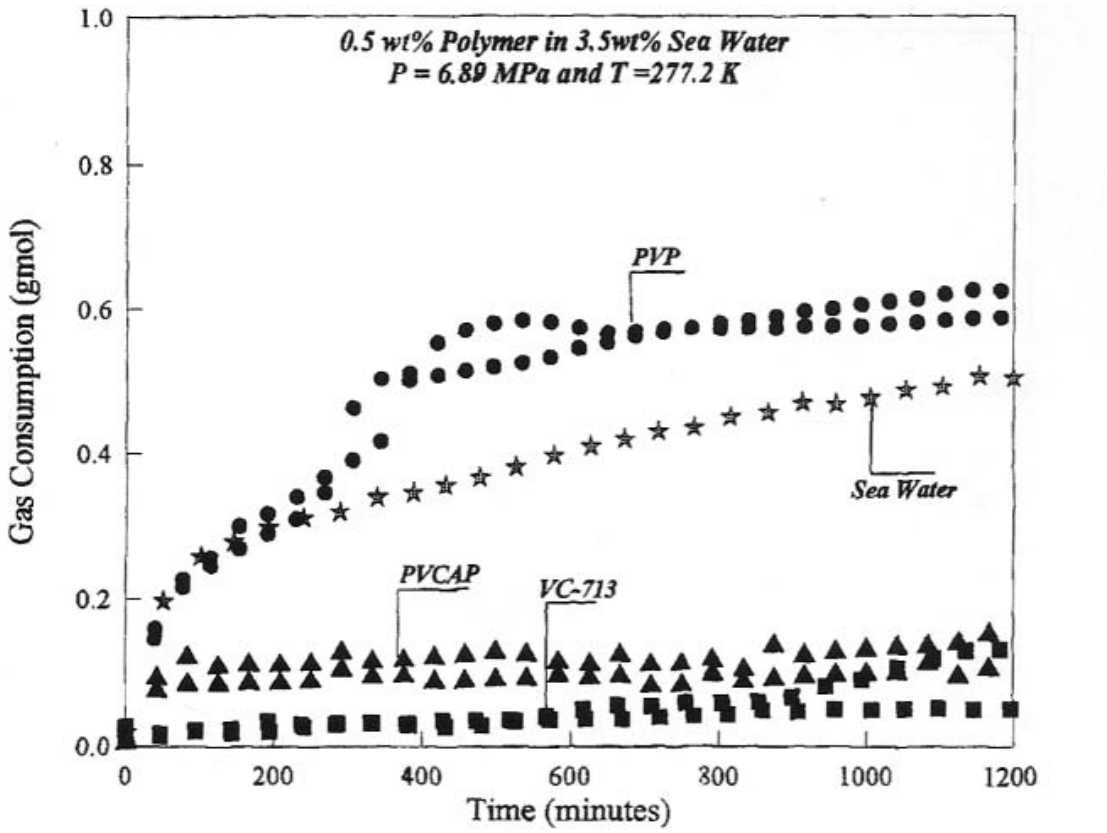

Figure 1.5.2 – Gas consumption of kinetic inhibitors (adapted from Lederhos et. al, 1996)

The concentration of the inhibitor affects its performance. Lederhos et al showed that the performance of PVCAP varied between 0.25-0.75 wt% at 277.2 K and 6890 kPa with 0.5 wt% resulting in the most effective inhibition results (Lederhos et. al, 1996). The performance of the inhibitor is also affected by the operating parameters and water quality. VC-713 polymer gave poor inhibiting performance at high pressures, while inhibited well at moderate pressures. Experiments done VC-713 showed that its inhibition performance deteriorated when the salt concentration decreased from 3.5 wt% to 0 wt% (Lederhos et. al, 1996).

Experiments were performed on the co-polymer poly(VP/VC) with different ratios of poly(VP/VC). Results revealed that the ratio of poly(VP/VC) affects the

inhibition performance. poly(VP/VC) with ratios of 25/75 produced the best inhibition results suggesting that the caprolactam group has more positive impact on inhibition (Lederhos et. al, 1996). Although the inhibition mechanism of these polymeric inhibitors is not yet well understood, it is believed that they are able to adsorb to the hydrate lattice because the lactam rings are similar in size to the faces of the hydrate cage and thus, can imbed themselves into the growing hydrate lattice (Lederhos et. al, 1996).

1.5.3 Antifreeze Proteins

Antifreeze proteins (AFP) are proteins that have an affinity for ice and are found in organisms such as fish, insects and plants. They are natural inhibitors that inhibit ice growth and therefore help the organisms survive freezing conditions. Around 35 years ago, AFPs were first discovered in the blood of the Antarctic fish (Zongchao and Davies, 2002). There are five different types of AFPs in fish, two in insects and three in in plants. AFPs in insects were reported to be more effective than the ones found in fish, while they are relatively weak in plants (Zongchao and Davies, 2002). Type I fish antifreeze proteins are produced by flounder and sculpin species of fish. Type I AFP is a small alanine-rich, amphipathic α-helix. It is the simplest of the fish AFPs and the one that has been most extensively used as a model system for trying to understand how these proteins bind to ice (Zongchao and Davies, 2002). The repeating structure of this peptide contains 37 amino acid residues (see Figure 1.5.3). Type I antifreeze proteins isolated from winter flounder were the only type of AFP tested in this work.

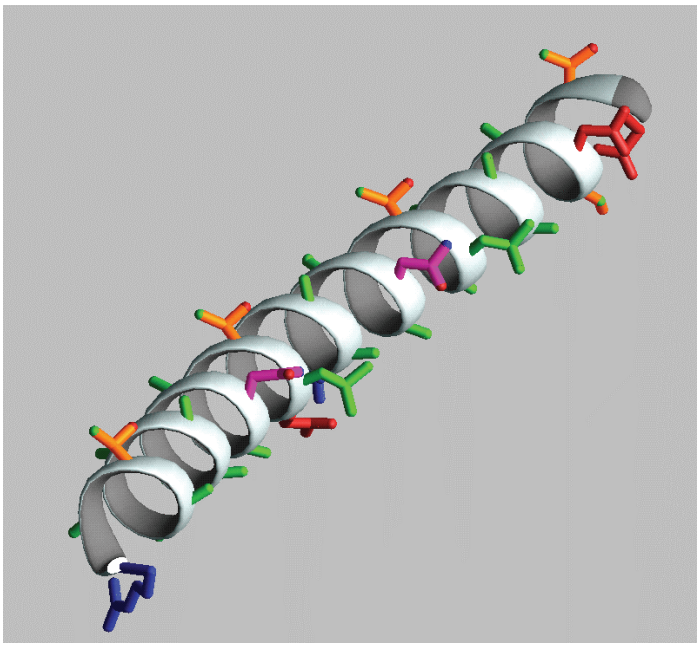

Figure 1.5.3 – Structure of Type I antifreeze protein (adapted from http://pout.cwru.edu)

In freezing climates fish produce AFPs to avoid freezing where they bind to the surface of the seed ice crystals to control their growth. AFPs restrict the addition of water to ice crystals causing a curvature in the ice front, which leads to an increase in the surface area. This decreases the tendency for water to add to the ice front, which results in the depression of the freezing point without amending a noticeable change in the melting point. The difference between the melting and freezing points is termed as thermal hysteresis (TH). It is caused by the interaction of AFP with ice and it is used to quantify the antifreeze activity (Zongchao and Davies, 2002). Studies have been conducted to observe the effect of antifreeze proteins on gas hydrates and they have shown that AFPs have an inhibiting effect on gas hydrate formation (Ripmeester, 2003).

1.6 Research Objectives

The first part of the project was to test how effective AFPs are as hydrate inhibitors and compare their performance with a classical inhibitor [poly(VP/VC)]. The second part of this project was to test polymers that have not been associated with hydrate formation and inhibition before and explore their effect on the kinetics of hydration formation. The polymers are poly(2-acrylamido-2-methyl-1-propane sulfonic acid), (P2A2MPSA) sodium salt and poly (acrylic acid), (PAA) sodium salt.

2 EXPERIMENTAL SET-UP, PROCEDURE AND METHODS

2.1 Apparatus

A schematic diagram of the apparatus used for all experiments is shown in Figure 3.1.1. A high-pressure stainless steel 316 crystallizer or reactor was designed and constructed specifically for these experiments. The reactor was designed to withstand 20 MPa and was equipped with two polycarbonate windows that allowed illumination and observation of the contents inside. The internal diameter of the reactor was 3" and the sides of the reactor were 1.75" thick. The internal volume of the reactor was 610 ml. The reactor was immersed in a temperature control bath that maintained the reactor and its contents at a constant temperature throughout each experiment. The temperature control bath contained a 50/50 volume mixture of water and ethylene glycol. The mixture inside the bath was cooled using an electric chiller (Neslab RTE 740), which was equipped with a digital temperature controller.

Liquid solutions were inserted and removed from the reactor by means of a sample port located at its base. The sample port was a 1/8" npt fitting connected with tubing to the outside of the temperature control bath. The pressure inside the reactor was monitored using a Rosemount 3051 Smart Pressure Transmitter with a range of 0-13780

kPa and an accuracy of 0.04% of the span. Gas was supplied to the reactor from a reservoir also immersed in the temperature control bath. A pneumatic control valve obtained from Rosemount was used to control the flow rate of gas into the reactor and maintained the pressure at a constant value throughout an experiment. To provide the controller with a more precise reactor pressure reading, a bias reactor kept at a constant pressure was immersed in the temperature control bath as well. The differential pressure between this bias reactor and the reactor was monitored using a Rosemount 3051 Smart Pressure Transmitter with a smaller range of 0-2000 kPa and an accuracy of 0.04% of span. The smaller range increased the precision of the pressure readings inside the reactor and allowed the controller to respond to changes in that pressure more readily.

A similar set-up was used to monitor the reservoir pressure in order to provide a precise measurement of the amount of gas leaving the reservoir and entering the reactor. This reading was used to calculate the number of moles of gas consumed during hydrate formation. Another bias reservoir kept at a constant pressure was immersed in the temperature control bath and kept at a constant pressure. The differential pressure between this bias reservoir and the main reservoir was monitored using a Rosemount 3051 Smart Pressure Transducer with a range of 0-2000 kPa. The overall pressure inside the bias was also monitored using a Rosemount 3051 Smart Pressure Transducer with a range of 0-13780 kPa. All readings were monitored using a Labview 7.1 (National Instruments) data acquisition system. This program recorded all pressure and temperature readings and saved them in a Microsoft Excel file. The temperatures of the main reservoir and the reactor gas phase and liquid phase were measured using platinum RTDs connected to a data acquisition system and were accurate to 0.5°C. Agitation inside the

reactor was achieved with the use of a magnetic stir bar coupled to a rotating magnet located underneath the temperature control bath. The magnet was rotated at approximately 800 rpm for every experiment to minimize the mass transfer resistances. (see Figure 2.1.1).

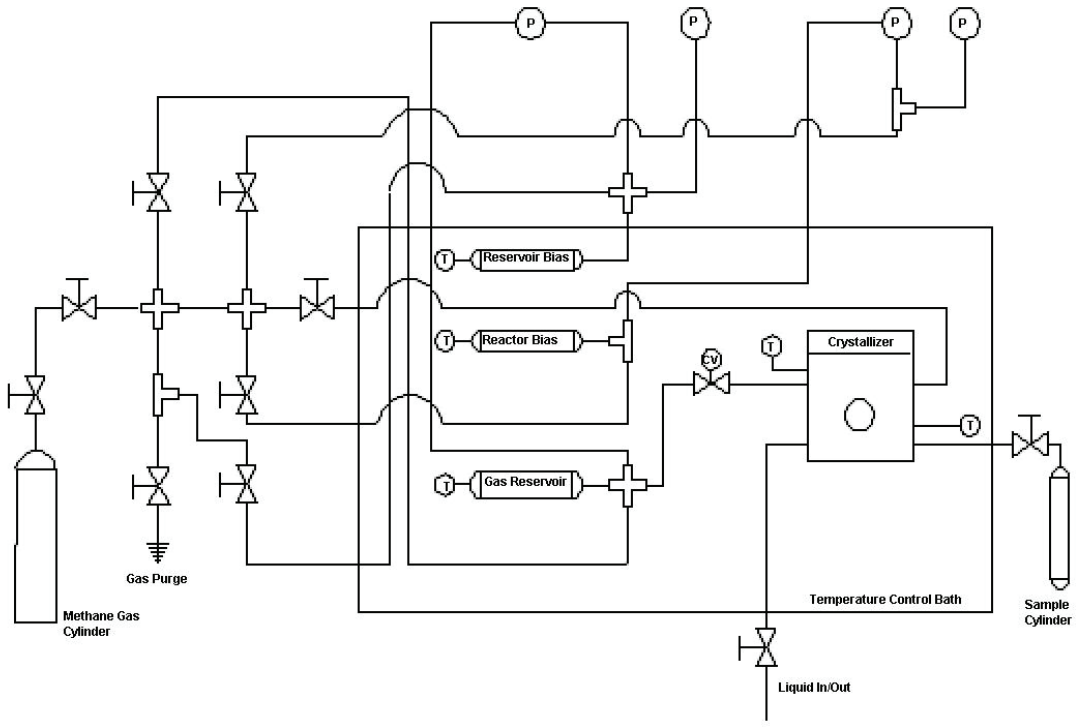

Figure 2.1.1 - Apparatus Schematic

2.2 Materials

The chemicals used during the experimental work were: antifreeze proteins, copolymer of VP/VCap, poly(2-acrylamido-2-methyl-1-propane sulfonic acid), sodium salt and poly(acrylic acid), sodium salt.

Purified fish Type I AFP from winter flounder (average molecular weight: 4000 g/mole) was purchased from A/F Protein Canada Inc. copolymer of VP/VCap (1:1 mole ratio of VP to VCap dissolved in H_2O, average molecular weight: 7000 g/mole) was

purchased from BASF. P2A2MPSA, sodium salt (average molecular weight: 800,000 g/mole was purchased from Scientific Polymer Products, Inc. PAA, sodium salt (average molecular weight: 2100 g/mole and 6000 g/mole) was purchased from Polysciences, Inc. (see Figure 2.2.1).

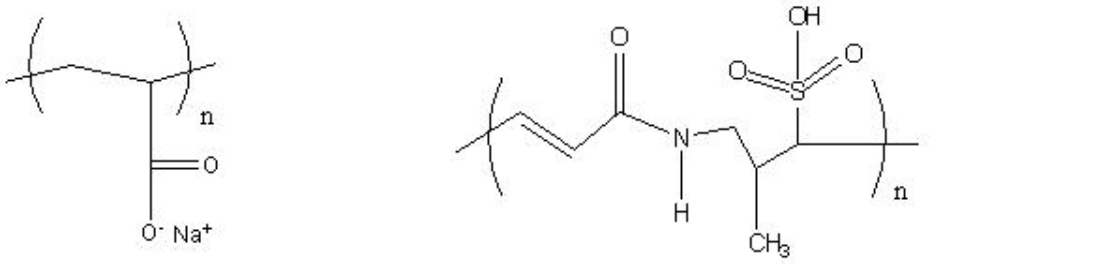

Poly(acrylic acid), soudium salt

Poly(2-acrylamido-2-methylpropane sulfonice acid), sodium salt

Figure 2.2.1– Chemical structure of Tested Polymers

All chemicals were dissolved in 250 ml of distilled and deionised water. The experiments were conducted in a methane-water system. The methane used was at ultra high purity levels and provided from MEGS.

2.3 Experimental Procedure

The experiments operating pressure ranges between 5800-8100 kPa and the temperature between 275.15-279.15 K. The experimental procedure can be divided into the following steps:

1. Injecting the solution
2. Pressurizing the system
3. Running the experiment
4. Terminating the experiment
5. Depressurizing the system
6. Cleaning the reactor.

2.3.1 Injecting the Solution

Before injecting the solution into the crystallizer, the purge line is opened to insure no pressure resistance is forced on the syringe that is used to insert the solution. Then a syringe is used to inject the solution throughout the sample port. After the solution is fully injected into the reactor, the purge line is closed and the reactor is pressurized up to about 500 kPa. The stirrer is then turned on.

2.3.2 Pressurizing the System

Prior to pressurizing, the stirrer inside the reactor must be turned off and all valves should be closed. Then the data acquisition system is turned on to monitor the pressure and temperature of the system. The next steps only progress after the reactor liquid temperatures reach the desired target. At this stage the control valve should be set on automatic and set to a set-point that insures that it remains closed until the experimental run starts. After the gas cylinder regulator valve is adjusted to the desired pressure, the outlet valves of the cylinder and the regulator are opened where the gas reaches the system main inlet valve at this point. The reactor and bias reactor inlet valves should be left open so that they reach equilibrium and get prepared to be pressurized simultaneously. The main inlet valve is then cracked open where the reactor and bias reactor start getting pressurized until the desired pressure is reached. Then the reactor valve is closed and a small push of gas is allowed to enter the reactor bias only in order to keep its pressure always slightly higher than the reactor pressure. Then all values are closed except the reservoir and reservoir bias. By crack opening the main inlet valve, both the reservoir and its bias start getting pressurized. The pressuring stops after the reservoir pressure is higher than the reactor pressure by at least 1000 kPa. After the desired pressure of the system is achieved, all valves are closed except the reactor inlet

and transducer isolation valves. The system is then left to equilibrate. The cylinder and regulator valves are then closed.

2.3.3 Running the Experiment

After the system pressure and temperature start to stabilize, the control valve is set at the appropriate set point. The experiment run is then started once the stirrer is trued on and the data acquisition system begins recording. After the stirrer is turned on, the gas will start dissolving into the solution and afterwards hydrates will start to form. The condition of the stirrer has to always be monitored because it can sometimes decouple, which will slow down or even stop the formation of hydrates and affect the experimental results.

2.3.4 Terminating the Experiment

The experiment run is usually considered done when all the solution forms hydrates and no liquid solution is observed through the window. The run can also be considered finished when mass transfer limitation is observed in the data acquisition system, which can be resulted by the stirrer moving limitations or decoupling. After the experimental run is considered over, the first step is to stop recording the data acquisition system. Then the stirrer is turned off and the depressurizing process can start. The set point of the control valve is set to 99.99% in order to make sure its wide shut.

2.3.5 Depressurizing the System

After the sitter is turned off, the reactor and bias reactor valves are opened. Then the purge valve is crack opened and the depressurizing process starts gradually where hydrates start decomposing. Depressurizing the reactor and its bias is stopped after the pressure of the reactor reaches around 1000 kPa. Then the reactor and bias reactor valves

are closed and the reservoir and bias reservoir valves are opened. Then the purge valve is crack opened again in order to depressurize the reservoir and its bias until the pressure within the reservoir reaches around 3000 kPa. Awareness has to be present while depressurizing the reactor and its bias to make sure the solution is not also purged with the gas. This can happen if rapid purging of the gas occurs, which leads to a huge temperature decrease as a result of the sudden pressure drop. This can lead to a massive hydrate formation within all parts of the reactor. The reactor purge line is located at the top part of the reactor. If the solution reaches the purge line during the depressurizing process, some the solution can get sucked out of the reactor, which is undesired. If the solution starts to expand and form hydrates close to the reactor outlet line, depressurizing has to be stopped until the solution starts to drop well below the outlet line. At some cases the temperature of the bath has to be raised in order to decompose the hydrates by temperature influence instead of pressure.

2.3.6 Cleaning the Reactor

The reactor is cleaned using deionized water only. Before starting the injection of water into the reactor, the purge valve has to be opened in order to insure that the pressure inside the reactor is less than 10 kPa. All other vales must be kept closed except the transducer isolation valve. The water is then injected into the reactor using a syringe until the water level reaches the top part of the window. The stirrer is then turned on at around 30% and the purge valve is closed. The reactor is then pressurized to approximately 600 kPa. The sample port valve is then opened to remove the water from the reactor. The above steps are repeated as many times as needed to insure that the reactor is cleaned well enough.

2.4 Method of Measurement and Calculation

After experiments are conducted, data is recorded into a MS Excel file. Then a plot of reservoir differential pressure and reactor liquid temperature vs. time is developed (see Figure 2.4.1).

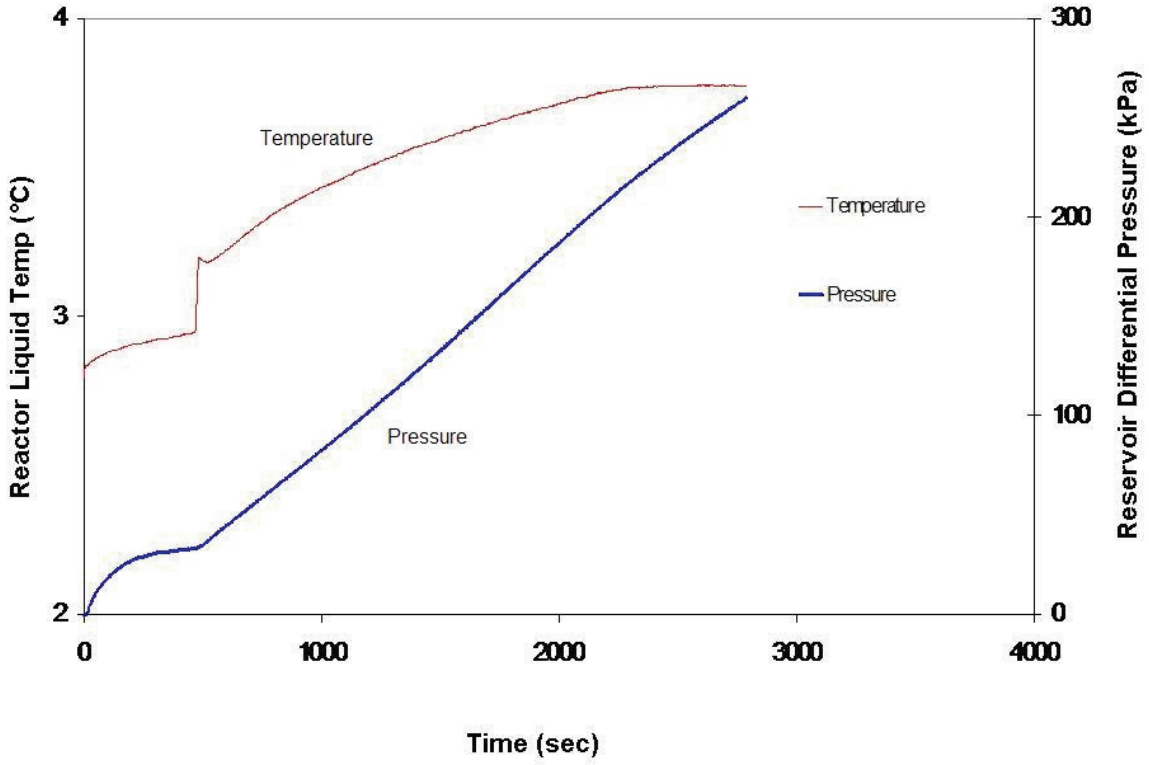

Figure 2.4.1 – Reservoir Pressure Drop and Reactor Liquid Temperature vs. Time

A Matlab program that uses the Trebble-Bishnoi equation of state (Trebble and Bishnoi, 1987) is then used to convert the reservoir pressure drop into moles. The moles calculated are the moles consumed during hydrate formation. A plot of moles consumed and reactor liquid temperature is then developed and the data is analyzed. The main parts of the data analysis are the nucleation time and growth period.

2.4.1 Nucleation Time Measurement

The nucleation time is measured during each hydrate formation experiment. It is defined as the time where the stirrer was turned-on in the reactor until hydrates are observed, which indicates that the growth period has started. For more accurate measurements, the nucleation time is determined after reviewing the recorded data and generated mole consumption plot. The reactor liquid temperature is useful to determine the nucleation time since a spike in the temperature is usually observed during the initial stage of growth (see Figure 1.4.1). Nucleation times are compared between experiments especially when inhibitors are used to check their effect on induction period.

2.4.2 Growth Measurement

The growth period is measured for every experimental run. Its starting point is considered as the point where a spike in the pressure differential and liquid reactor temperature is noticed. The end of the growth period is considered as the point where the profile of growth curve starts changing, which is an induction that the stirrer in the reactor decoupled and that disturbs the growth. The growth periods measured for deionized water were considered as a reference point. Then the growth periods measured for the other solutions were compared to the reference in order to determine their effect on growth. By implanting this method, the tested solutions were classified as inhibitors or promoters and their degree of effectiveness was determined.

3 RESULTS AND DISCUSSION

3.1 The Effect of Kinetic Inhibitors on Hydrate Growth Profile

After conducting several kinetic experiments with deionized water and different kinetic inhibitors, it was observed that the growth profile for a system that included a kinetic inhibitor was different than the experiments done with deionized water alone.

This observation is clearly shown in Figure 3.1.1 that includes the mole consumption curves for deionized water and poly(VP/VC) at approximately 277.15 K, 6500 kPa and a concentration of 0.1 wt%. The plot in Figure 3.1.1 clearly demonstrates that poly(VP/VC) inhibits growth. More importantly, the plot shows the difference between the hydrate formation growth curves of deionized water and poly(VP/VC).

Figure 3.1.2 illustrates a typical gas mole consumption curve for a system that includes a kinetic inhibitor. Region A represents the dissolution and nucleation period, which continues until stable nuclei are formed. Region B begins at the turbidity point and represents the initial growth period. It can be noticed that the growth curve does not follow a linear profile. In that region, stable nuclei crystals grow but their growth is slower and non-linear due to the presence of a kinetic inhibitor. The inhibitor adsorbs to the surface of the hydrate particle and decreases the available area for hydrate formation. This decrease in hydrate surface area affects the term $\frac{1}{K_r A_p}$ and causes it to become large and significant when compared to $\frac{1}{K_l A_i}$ so that the global reaction rate constant becomes dominated by the reaction resistance term, therefore $K^* = K_r A_p$. The intrinsic rate constant K_r depends only on the temperature and composition and those two factors are being held constant during the experiment. The surface area of the hydrate particle, A_p, is not constant since it increases during the experiment. Since A_p is not constant and varies with time, the curve in region B cannot be linear. It has been shown by a population balance that A_p is a quadratic function of time (Bergeron and Servio, 2007), (Kane et. Al, 1974), which explains why the curve seems to follow the path of a second order behavior as seen in Figure 3.1.2. As time progresses, the surface area of the hydrate

particles becomes large enough that the $\frac{1}{K_l A_i}$ term becomes more significant than the $\frac{1}{K_r A_p}$ term. The liquid side resistance to mass transfer now dominates the global reaction rate constant, therefore $K^* = K_l A_i$. The diffusion rate constant K_l, depends on the hydrodynamic conditions as well as the temperature of the system, which are both held constant. The area at the gas-liquid interface, A_i is also constant. Therefore, the term $\frac{1}{K_l A_i}$ may be considered to be independent of time and hydrate growth. In response to this change in the dominating resistance, the growth rate follows a linear profile as shown in region C of Figure 3.1.2. The region beyond C is the growth that occurs after mass transfer limitations within the system become significant. This occurs when the reactor is saturated with hydrates and the system is no longer agitated in a controlled manner. The region beyond C is not used during the analysis of the results.

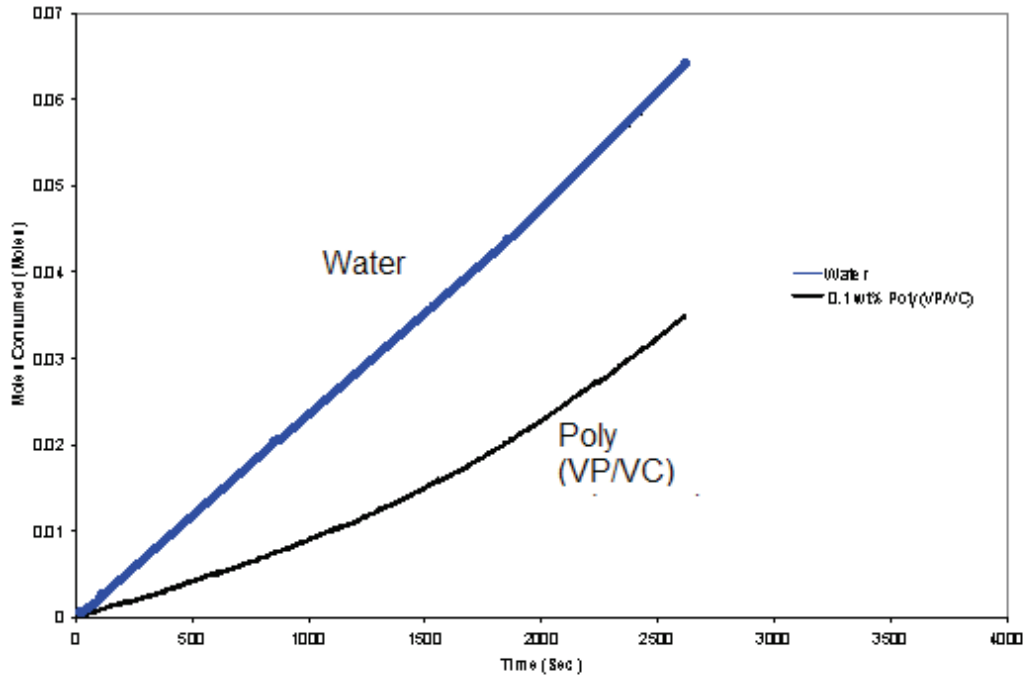

Figure 3.1.1– Mole consumption of deionized water and poly(VP/VC) at 277.15 K and 6500 kPa

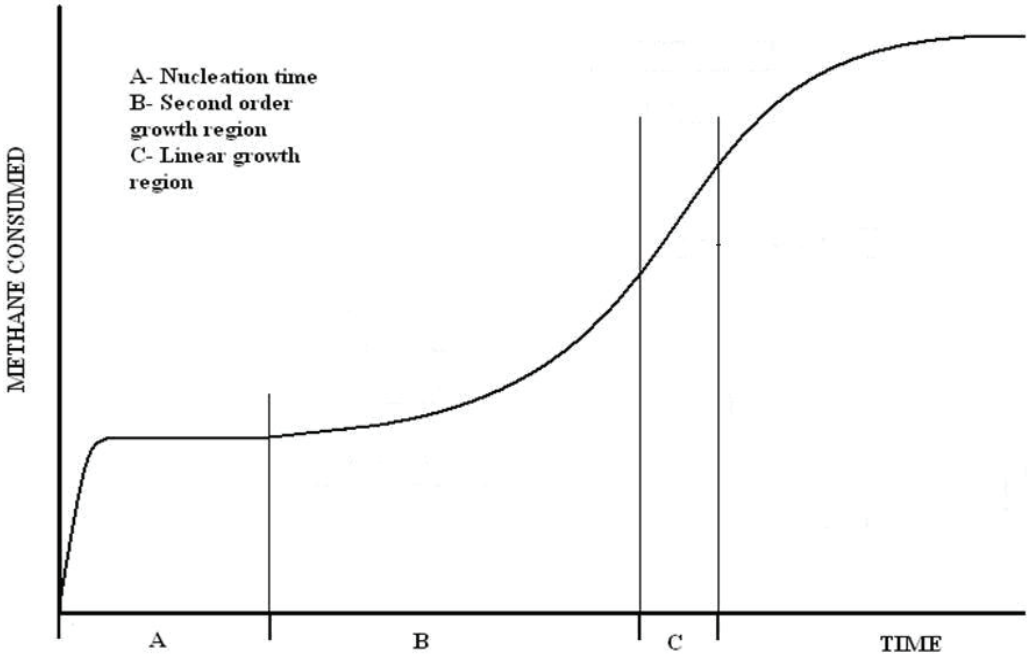

Figure 3.1.2– Mole Consumption Plot for System with a Kinetic Inhibitor

3.2 Inhibitor Performance Comparison

Experiments were conducted at conditions within the thermodynamic hydrate forming region as the equilibrium hydrate conditions are approximately at 277.15 K and 3800 kPa. The experimental conditions were kept constant at a temperature of 277.15 K (± 0.3°C) and a pressure of 6500 kPa (± 26 kPa). The AFP concentration used during the experiments was 0.0175 mM, which is equivalent to 0.007 wt%. Three different concentrations were tested on poly(VP/VC), which were 0.005 mM (0.0035 wt%), 0.01 mM (0.007wt%) and 0.25 mM (0.1wt%). Three experiments were run at each concentration and the average mole consumption curves were generated. The performance of each solution was analyzed by comparing these curves to the average mole consumption curve of deionized water alone, which was tested at the same experimental temperature and pressure conditions.

Figure 3.2.1 illustrates the average mole consumption curves for deionized water, poly(VP/VC) and AFP at 277.15 K and 6500 kPa. As seen from the plot all the growth curves of poly(VP/VC) and AFP are lower than water, which indicates a slower rate of growth and therefore kinetic inhibition. The plot also shows that the inhibition activity varied for poly(VP/VC) at different concentrations. An interesting finding is that at a concentration of 0.007 wt%, both AFP and poly(VP/VC) had the same number of moles consumed (0.0209 moles) after 15 minutes of hydrate growth. This value represented a 24% decrease in hydrate growth compared to the growth after 15 minutes in deionized water alone. It was also found that poly(VP/VC) had the most significant effect on growth at the highest concentration of 0.1 wt% where the moles consumed after 15 minutes was the lowest (0.0095 moles) of the conditions tested. By comparing this mole

consumption value with deionized water, it was found that the growth value was 65% lower. This indicates that the inhibitor performance improved by approximately 41% after its weight concentration was increased by a factor of 14. Table 3.2.1 illustrates all the experimental conditions used for this work and also provides the number of moles consumed, growth inhibition and absolute average deviation for the number of moles consumed after 15 minutes of the growth period.

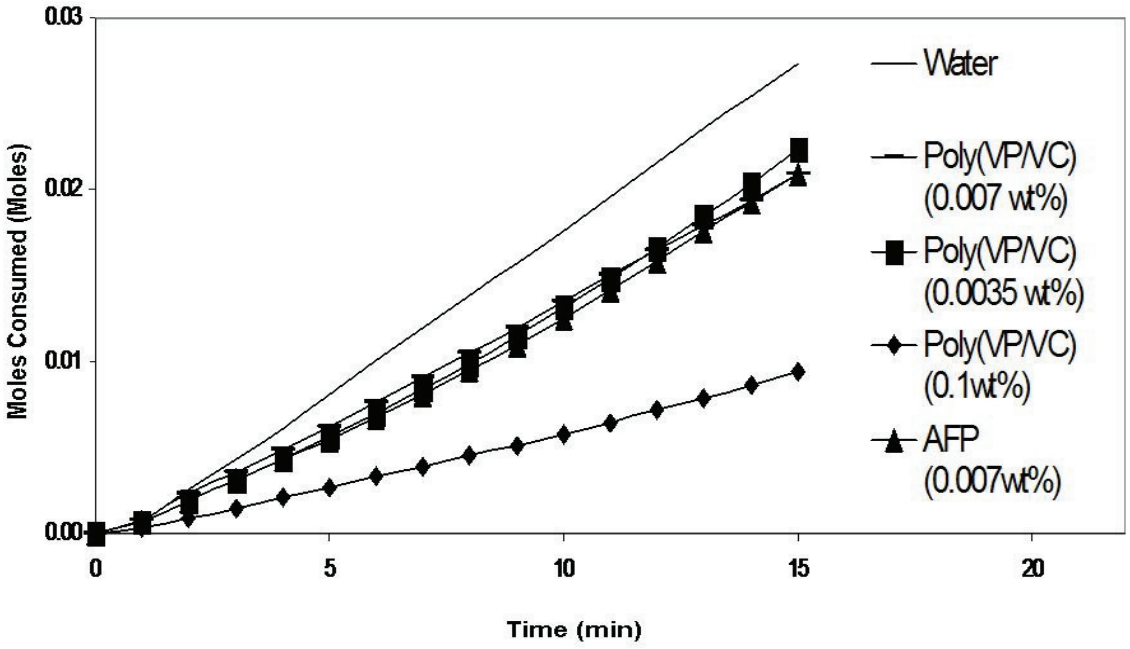

Figure 3.2.1– Average mole consumption of AFP & poly(VP/VC) at 277.15 K (equilibrium pressure ≈ 3800 kPa) and 6500 kPa

Table 3.2.1 – Experimental Conditions and percentage reduction of growth due to inhibition % after 15 minutes of experimental run

#	Solution Name	Conc. (wt%)	Avg. Temp (K)	Avg. Press (kPa)	# of Replicates	Inhibition %	Moles	Moles Abs. Avg. Dev.
1	Deionized Water	N/A	275.05	5807	3	N/A	0.0355	1.11E-03
2	AFP	0.0070	275.45	5831	2	11	0.0315	1.44E-03
3	Poly(VP/VC)	0.0035	275.05	5815	2	49	0.0183	1.35E-04
4	Deionized Water	N/A	277.15	5814	3	N/A	0.0249	9.65E-03
5	AFP	0.0070	277.45	5817	2	25	0.0188	7.74E-03
6	Poly(VP/VC)	0.0035	277.05	5799	2	37	0.0158	5.93E-03
7	Deionized Water	N/A	276.95	6498	3	N/A	0.0274	8.94E-04
8	AFP	0.0070	276.85	6500	3	24	0.0209	2.05E-03
9	Poly(VP/VC)	0.0035	276.95	6486	3	19	0.0223	3.20E-04
10	Poly(VP/VC)	0.0070	277.15	6502	3	24	0.0209	2.78E-04
11	Poly(VP/VC)	0.1000	277.15	6512	3	65	0.0095	5.79E-04
12	Deionized Water	N/A	277.15	7181	3	N/A	0.0327	4.9-3
13	AFP	0.0070	277.65	7169	2	-26	0.0413	1.57E-04
14	Poly(VP/VC)	0.0035	277.05	7201	2	21	0.0258	3.00E-03
15	Deionized Water	N/A	279.05	7401	1	N/A	0.0519	N/A
16	AFP	0.0070	279.65	7424	3	33	0.0349	1.64-3
17	Poly(VP/VC)	0.0035	279.25	7439	3	49	0.0267	4.38E-03

3.3 Effect of Pressure and Temperature on Hydrate Growth

Another set of experiments were conducted at conditions within the thermodynamic hydrate forming region where the temperature was kept constant at 277.15 K (± 0.5°C) while the pressure was examined at three different values: 5800 kPa, 6500 kPa and 7200 kPa (± 31 kPa). The AFP concentration used during the experiments was 0.007 wt%, while the concentration of poly(VP/VC) was 0.0035wt%. The average number of moles consumed was calculated for every solution at each experimental condition. Table 3.2.1, shows the number of experimental replicates for each solution and the operating conditions.

The average mole consumption curves for poly(VP/VC) and AFP at the three different pressure conditions is plotted in Figures 3.2.1, 3.3.1 and 3.3.2. The bar chart in Figure 3.3.5 summarizes the results of these experiments where the percentage reduction in hydrate growth due to kinetic inhibition was calculated for poly(VP/VC) and AFP. This was done by comparing the number of moles consumed after 15 minutes of hydrate growth with the inhibitor runs to the number of moles consumed after 15 minutes with deionized water alone. The results show that the reduction in hydrate growth was the highest at the lowest pressure of 5800 kPa. The growth reduction with poly(VP/VC) was found to be approximately 37% while it was 25% for AFP. At the highest pressure of 7200 kPa, the growth reduction in the poly(VP/VC) experiments was around 21%, while AFP had a growth rate higher than deionized water by 26% (see Table 3.2.1). This suggests that AFPs may act as hydrate growth promoters at higher pressures.

The effect of temperature on hydrate growth inhibition can be seen in Figures 3.3.2, 3.3.3, 3.3.4, 3.3.6 and 3.3.7. Figure 3.3.2 illustrates the average mole consumption

curves for poly(VP/VC) and AFP at approximately 277.15 K (± 0.5°C) and 7200 kPa (± 31 kPa). Figure 3.3.3 shows the average mole consumption curves for poly(VP/VC) and AFP at 279.15 K (± 0.5°C) and 7400 kPa (± 39 kPa), while Figure 3.3.4 shows the average mole consumption curves for poly(VP/VC) and AFP at 275.15 K (± 0.3°C) and 5800 kPa (± 31 kPa). The bar charts in Figure 3.3.6 and Figure 3.3.7 summarize the results of the temperature effect on hydrate growth. The growth inhibition for AFPs was better at higher temperatures as seen from Figures 3.3.6 and 3.3.7. This concludes that AFPs inhibit more effectively at a lower hydrate formation driving force (higher temperatures and lower pressures). For poly(VP/VC) the same conclusion can not be made. At the pressure of 7200-7400 kPa, the growth inhibition was more effective at the higher temperature of 279.15 K (see Figure 3.3.6), but at 5800 kPa, the growth inhibition was more effective at the lower temperature of 275.15 K (see Figure 3.3.7).

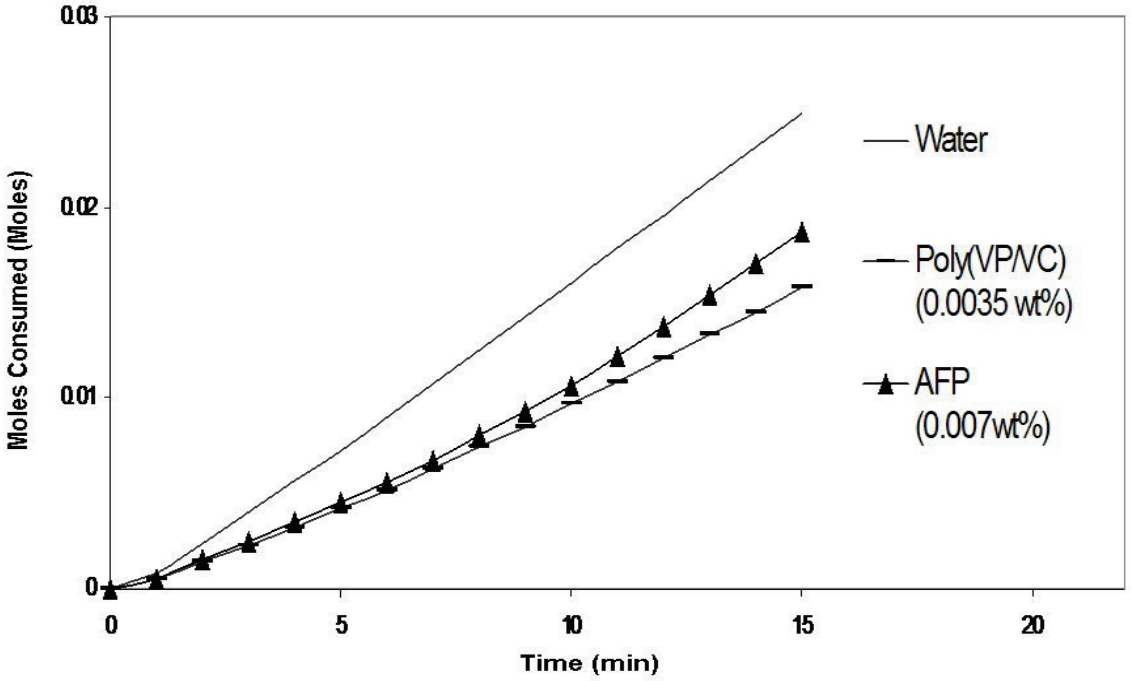

Figure 3.3.1– Average mole consumption of AFP & poly(VP/VC) at 277.15 K (equilibrium pressure ≈ 3800 kPa) and 5800 kPa

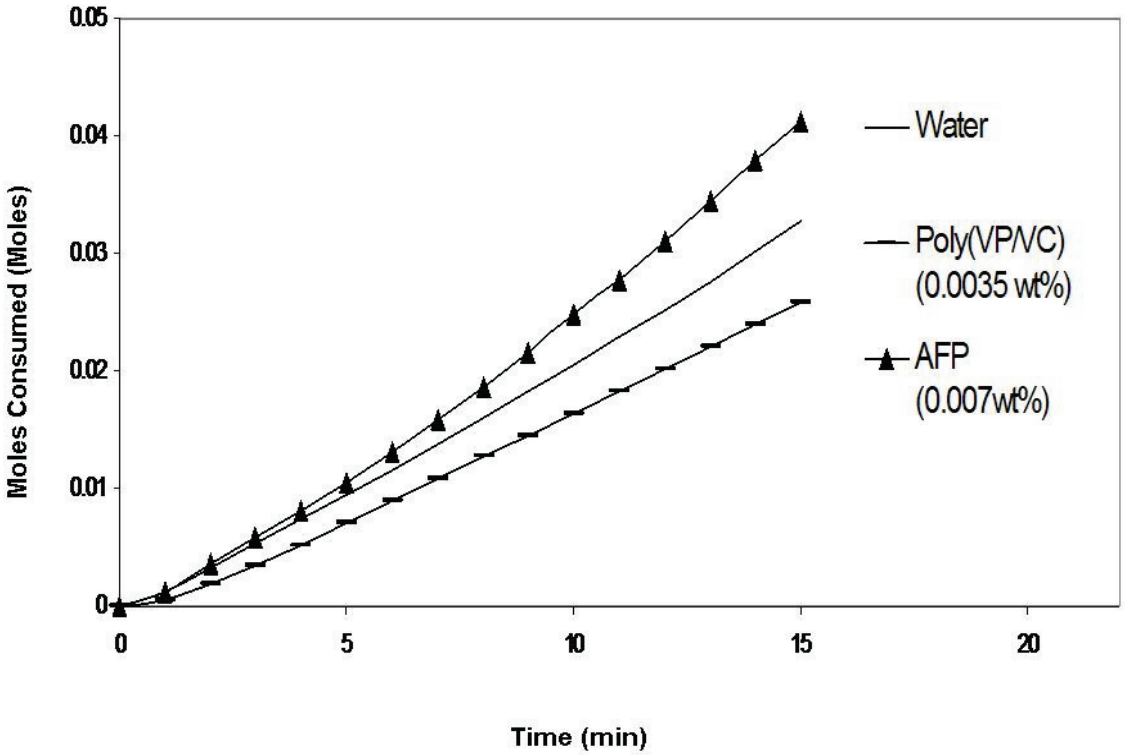

Figure 3.3.2– Average mole consumption of AFP & poly(VP/VC) at 277.15 K (equilibrium pressure ≈ 3800 kPa) and 7200 kPa

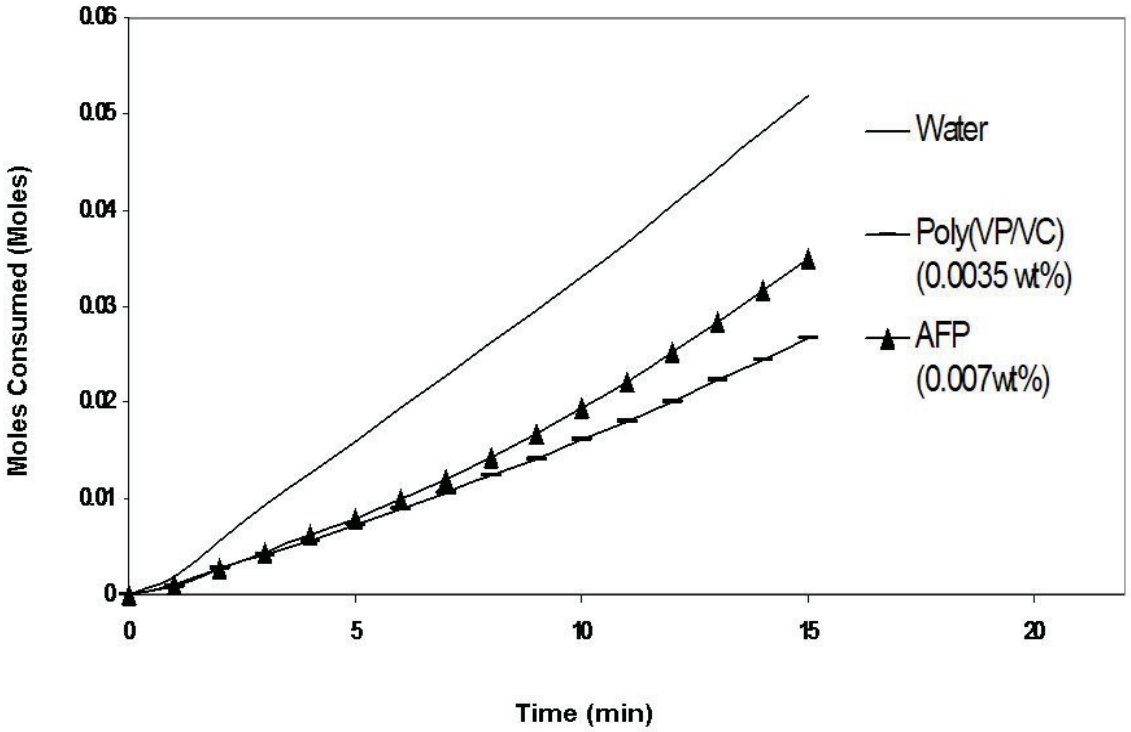

Figure 3.3.3– Average mole consumption of AFP & poly(VP/VC) at 279.15 K (equilibrium pressure ≈ 4700 kPa) and 7400 kPa

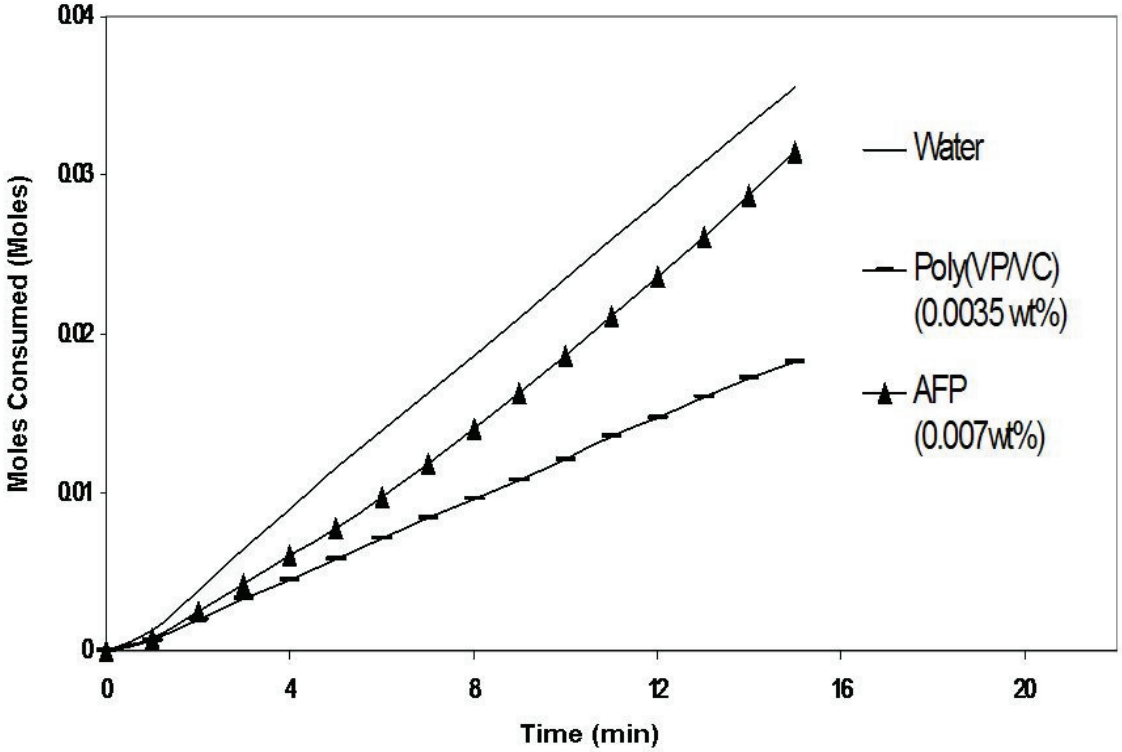

Figure 3.3.4 – Average mole consumption of AFP & poly(VP/VC) at 275.15 K (equilibrium pressure ≈ 3400 kPa) and 5800 kPa

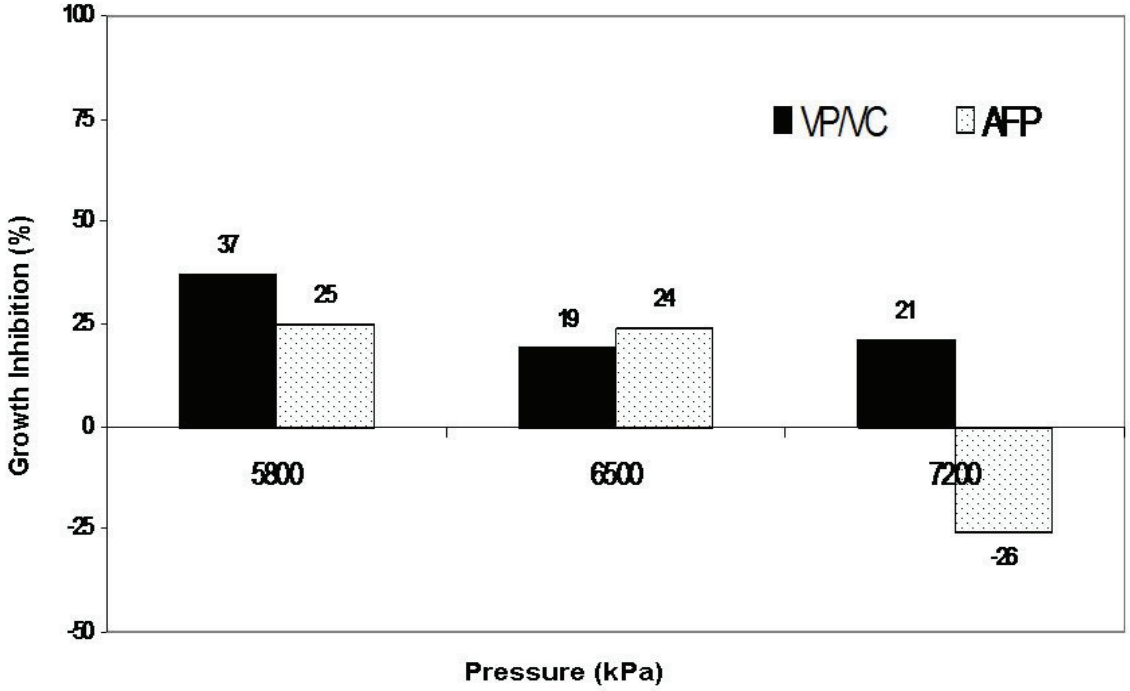

Figure 3.3.5 – Growth inhibition after 15 minute experimental run for poly(VP/VC) and AFP at 277.15 K and 5800, 6500 and 7200 kPa

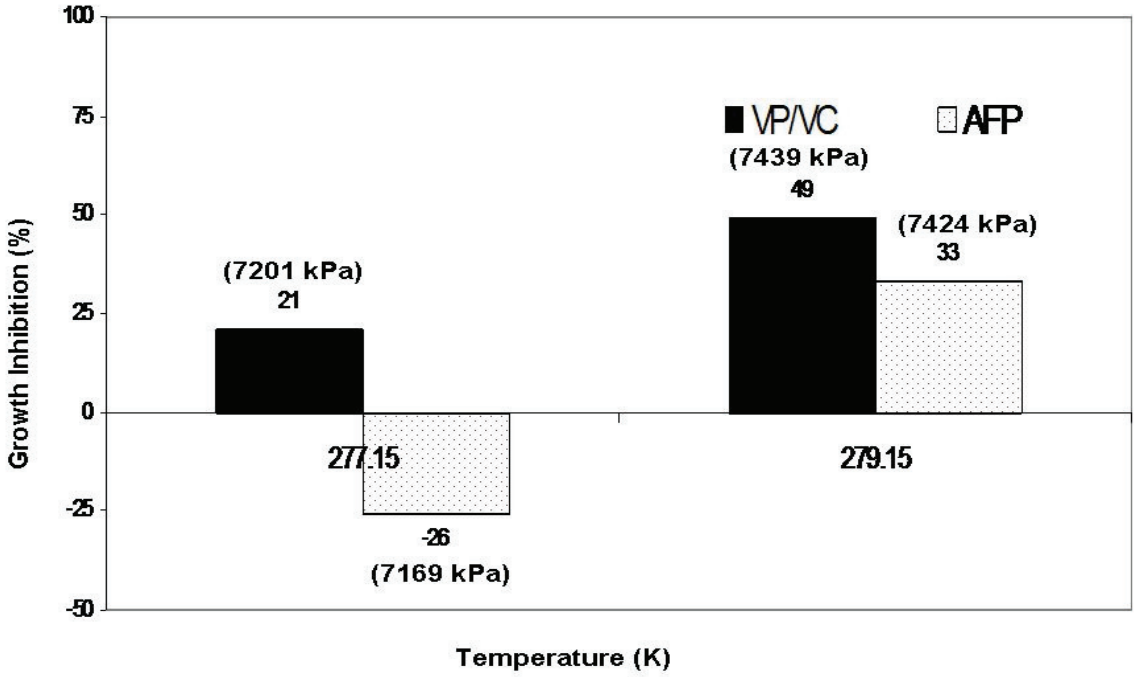

Figure 3.3.6– Growth inhibition after 15 minute experimental run for poly(VP/VC) and AFP at around 7200-7400 kPa and 277.15 and 279.15 K

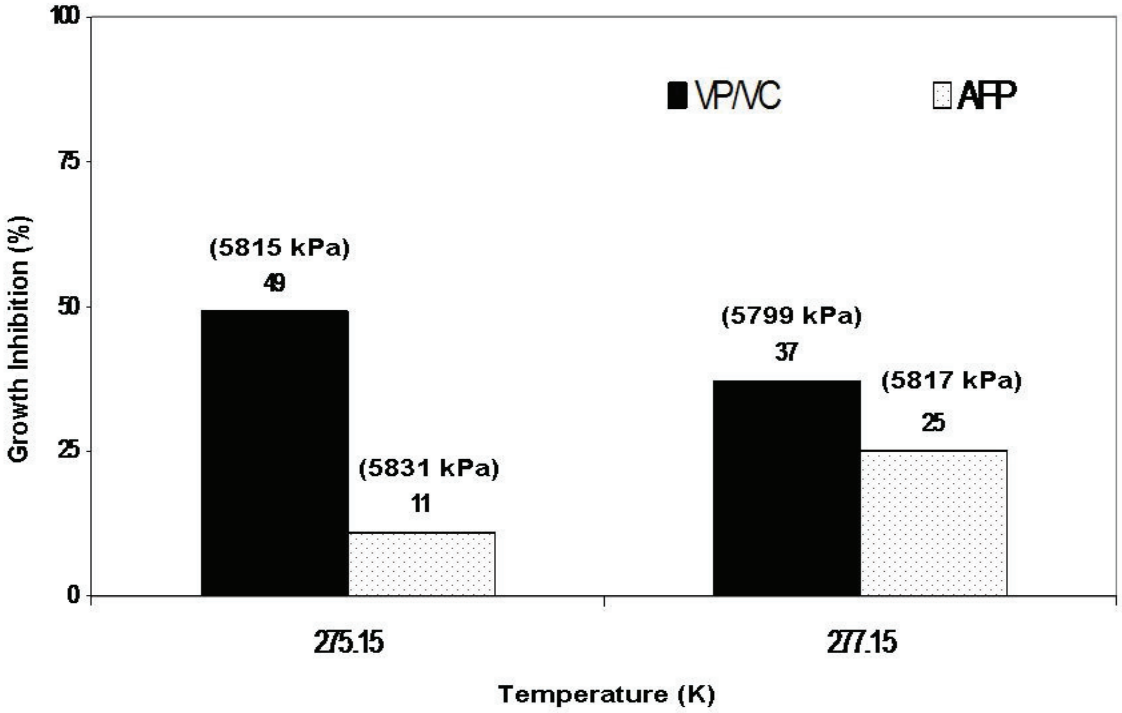

Figure 3.3.7– Growth inhibition after 15 minute experimental run for poly(VP/VC) and AFP at approximately 5800 kPa and 275.15 and 277.15 K

3.4 Testing the Effect of New Polymers on Hydrate Growth

The two polymers that were tested are poly(2-acrylamido-2-methylpropane sulfonic acid) (P2A2MPSA), sodium salt and poly(acrylic acid) (PAA), sodium salt, which were described in section 3.2 (see Figure 3.2.1). The objective of the tests was to determine their effect on hydrate growth.

3.4.1 Poly(2- acrylamido-2-methylpropane sulfonic acid), sodium salt

Experiments were conducted at a constant of temperature of 277.15 K (± 0.3°C) and three different pressures of 5800 kPa (±22 kPa), 6500 kPa (± 15 kPa) and 7200 kPa (± 48 kPa). The polymer concentration used during the experiments was 0.007 wt%. Three experimental replicates were conducted at each pressure condition. Figures 3.4.1, 3.4.2 and 3.4.3 include the gas mole consumption with the presence of that polymer at the

three different pressures. It can be seen from the plot in Figure 3.4.1 that growth rate with the presence of the polymer was higher than deionized water, which indicates hydrate growth promotion. This observation is clearer in Figure 3.4.2 at the higher pressure of 6500 kPa and at 7200 kPa where the growth was the highest as seen in Figure 3.4.3.

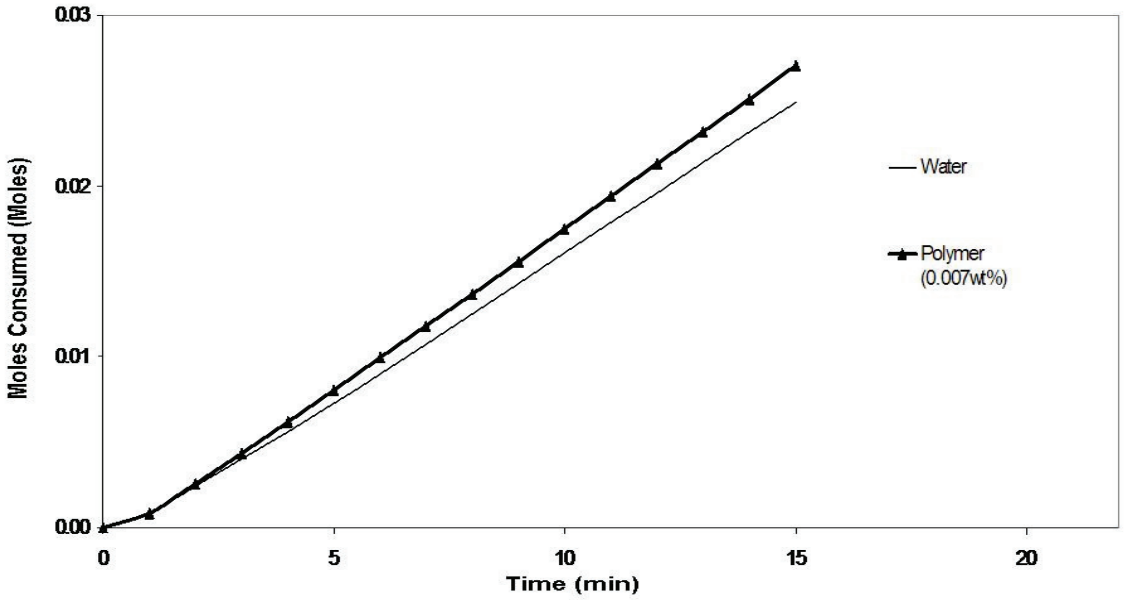

Figure 3.4.1– Average mole consumption of Poly(2- acrylamido-2-methylpropane sulfonic acid), sodium salt at 277.15 K and 5800 kPa

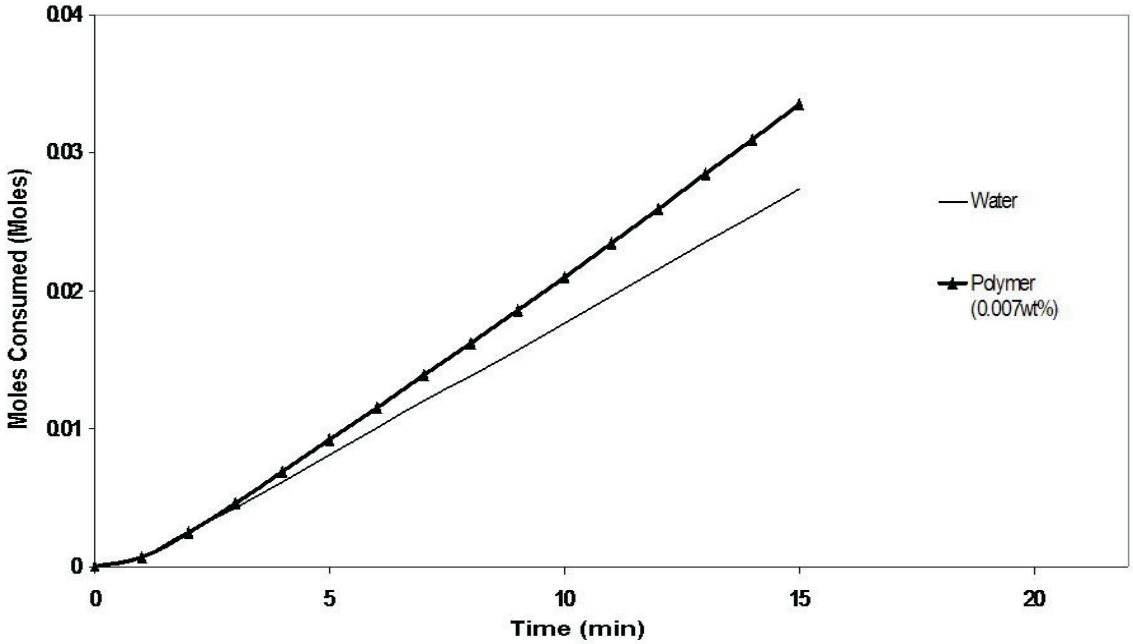

Figure 3.4.2– Average mole consumption of Poly(2- acrylamido-2-methylpropane sulfonic acid), sodium salt at 277.15 K and 6500 kPa

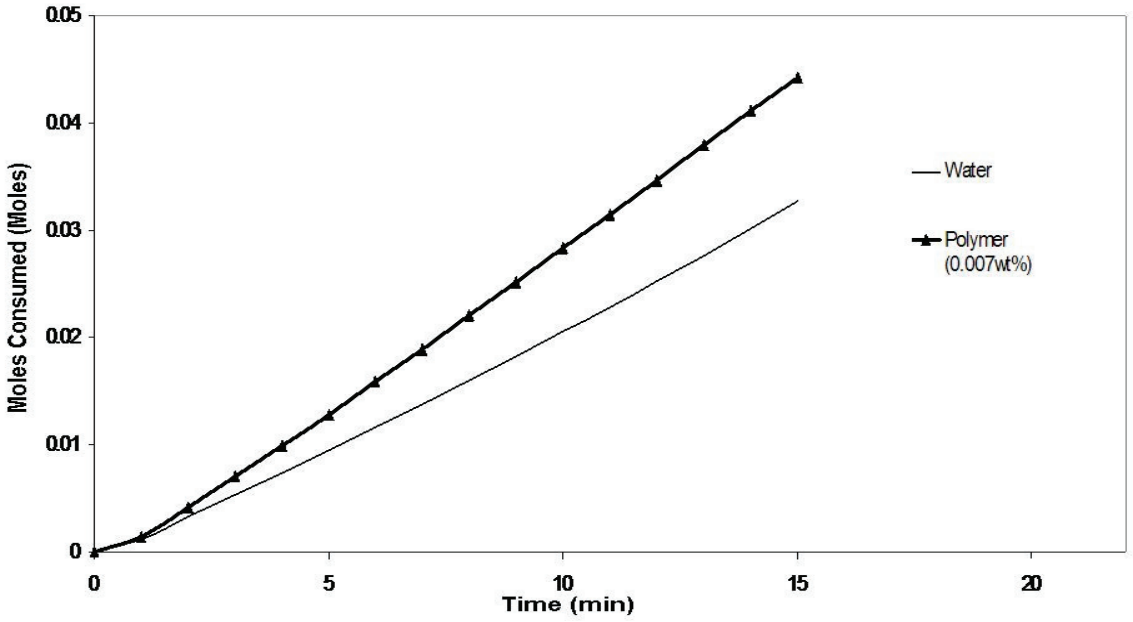

Figure 3.4.3– Average mole consumption of Poly(2- acrylamido-2-methylpropane sulfonic acid), sodium salt at 277.15 K and 7200 kPa

The bar charts in Figure 3.4.4 illustrate the percent increase in the hydrate growth for the polymer compared to deionized water after 15 minutes of the hydrate growth

period. This was done by comparing the number of moles consumed after 15 minutes of hydrate growth with the polymer runs to the number of moles consumed after 15 minutes with deionized water alone. The bar charts clearly show that at the highest pressure driving force (7200 kPa), the increase in hydrate growth was maximum at 35%. This concludes that that this polymer promotes hydrate growth and this promotion is enhanced with increasing the pressure at 277.15 K. Table 3.4.1 illustrates all the experimental conditions used for this work and also provides the number of moles consumed, growth increase percentage and absolute average deviation for the number of moles consumed after 15 minutes of the growth period.

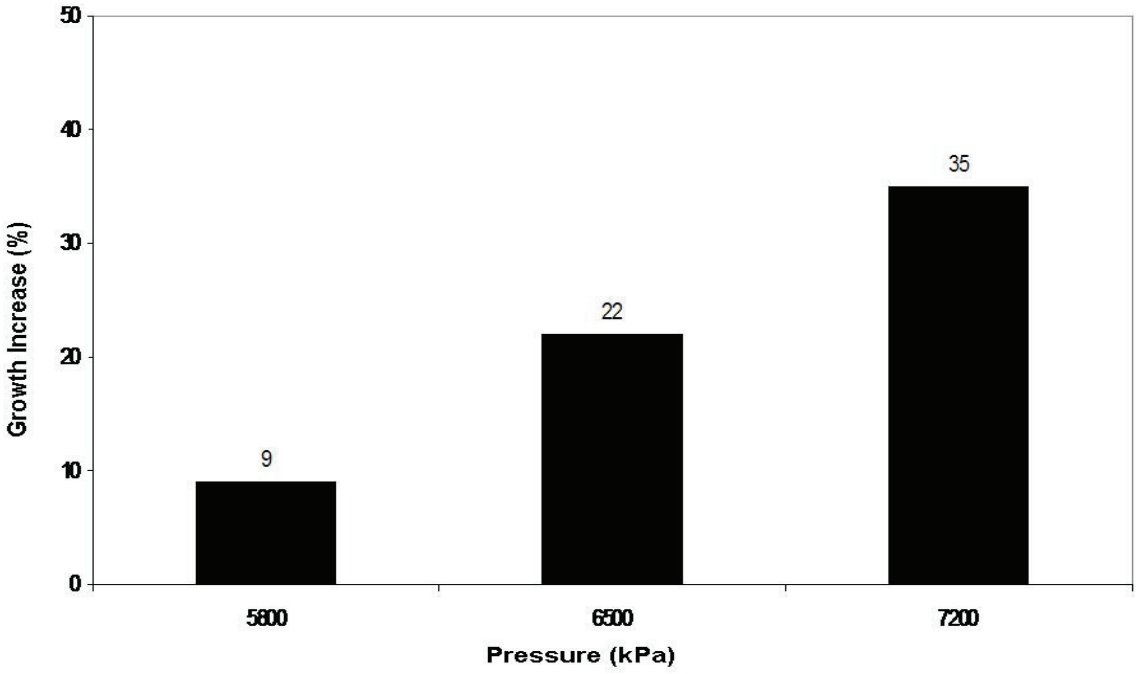

Figure 3.4.4 – Growth increase after 15 minute experimental run for Poly(2- acrylamido-2-methylpropane sulfonic acid), sodium salt at approximately 277.15

Table 3.4.1– Experimental Conditions and percentage increase of growth due to promotion % after 15 minutes of experimental run for P2A2MPSA

#	Solution Name	Conc. (wt%)	Avg. Temp (K)	Avg. Press (kPa)	# of Replicates	Growth Inc. (%)	Moles	Moles Abs. Avg. Dev.
1	Deionized Water	N/A	277.15	5813	3	N/A	0.0249	9.65E-04
2	P2A2MPSA	0.007	277.15	5817	3	9	0.0271	1.85E-03
3	Deionized Water	N/A	276.95	6498	3	N/A	0.0274	8.94E-04
4	P2A2MPSA	0.007	277.05	6504	3	22	0.0335	4.67E-04
5	Deionized Water	N/A	277.05	7181	3	N/A	0.0328	4.88E-03
6	P2A2MPSA	0.007	277.15	7212	3	35	0.0442	2.41E-03

3.4.2 Poly(acrylic acid), sodium salt

Experiments were conducted at a constant of temperature of 277.15 K (± 0.2°C) and pressure of 6500 kPa (± 14 kPa). The polymer was tested at two different concentrations (0.1 wt% and 0.5 wt%) in order to determine the effect of concentration on their performance. Also the polymer was tested at two different molecular weights (2100 g/mole and 6000g/mole) to verify the effect of molecular weight on hydrate growth.

As seen from the growth curves in Figure 3.4.5 and Figure 3.4.6, the polymer was promoting the hydrate growth. It can also be seen from the curves of the two figures that the growth was more aggressive at the higher concentration. For the polymer with the higher molecular weight of 6000 g/mole and lower concentration of 0.1 wt%, the growth curve almost overlaps with the growth curve of deionized water and makes it difficult to show the growth curve for water clearly (see Figure 3.4.6).

The bar charts in Figure 3.4.7 illustrate the percent increase in the hydrate growth for the polymer compared to deionized water after 6 minutes of the hydrate growth period. This was done by comparing the number of moles consumed after 6 minutes of

hydrate growth with the polymer runs to the number of moles consumed after 6 minutes with deionized water alone. The bar chart clearly shows that the increase in hydrate growth was maximum (140%) for the polymer with lower molecular weight and higher concentration. The increase in growth was not even present (0%) for the polymer with the higher molecular weight and lower concentration. This suggest that at the experimental conditions, the hydrate growth promotion for poly(acrylic acid), sodium salt is enhanced at lower molecular weights and higher concentrations. Table 3.4.2 illustrates all the experimental conditions used for this work and also provides the number of moles consumed, growth increase percentage and absolute average deviation for the number of moles consumed after 6 minutes of the growth period.

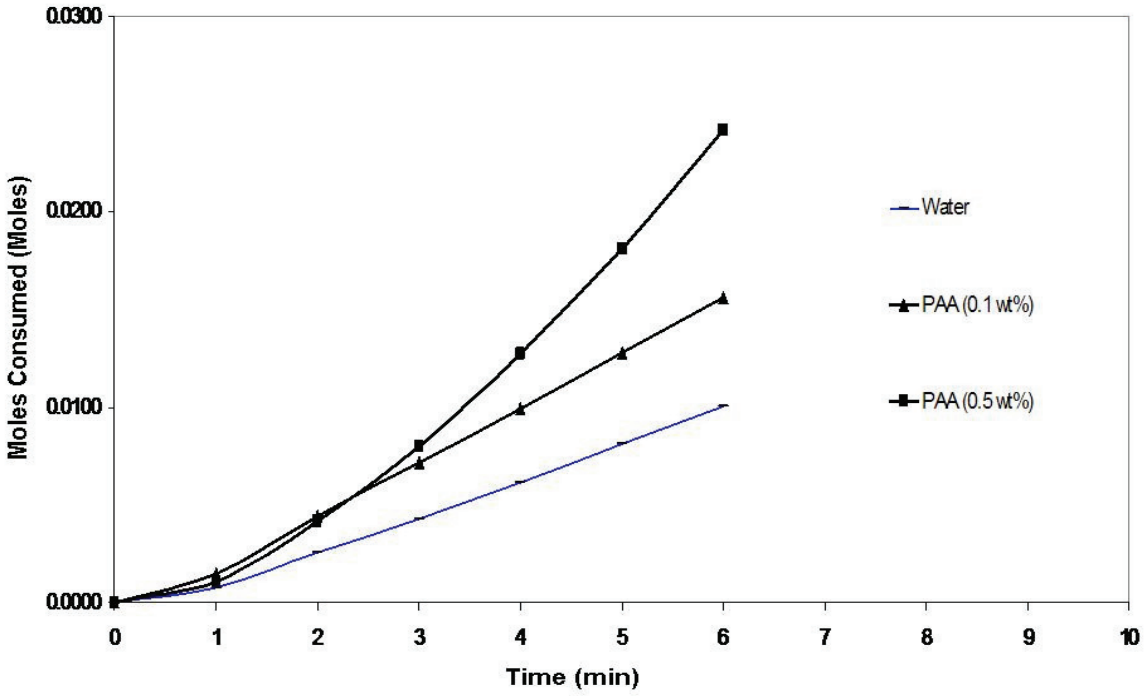

Figure 3.4.5– Average mole consumption of Poly(acrylic acid), sodium salt at 277.15 K, 6500 kPa and molecular weight of 2100 g/mole

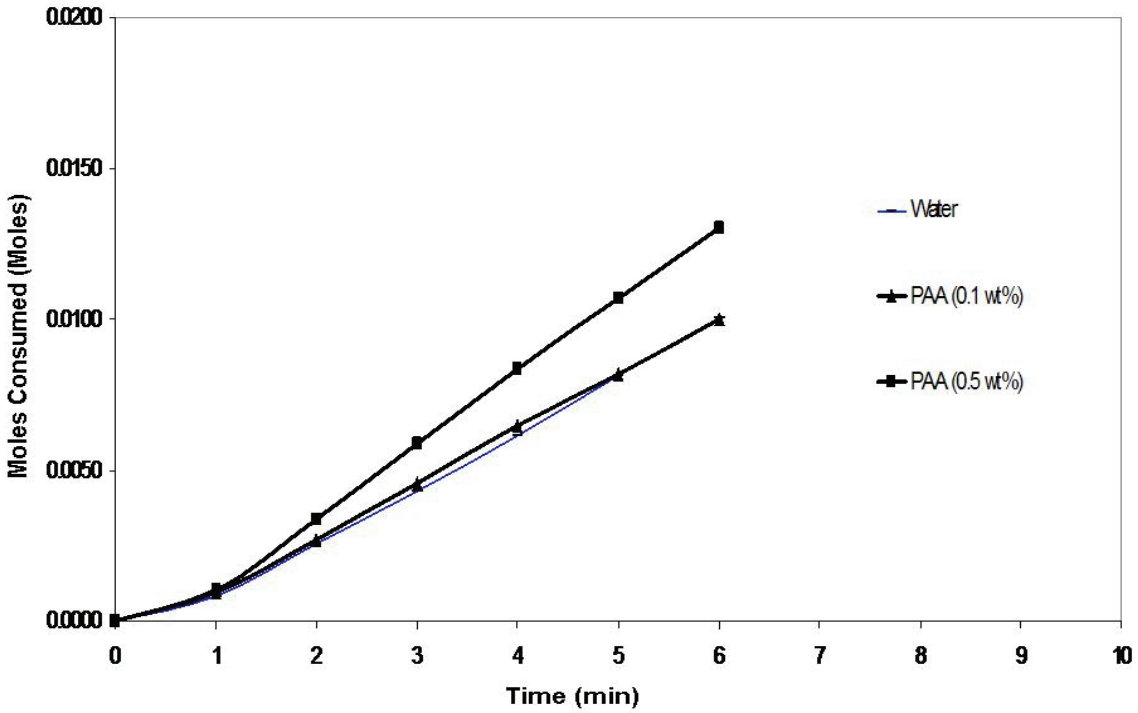

Figure 3.4.6– Average mole consumption of Poly(acrylic acid), sodium salt at 277.15 K, 6500 kPa and molecular weight of 6000 g/mole

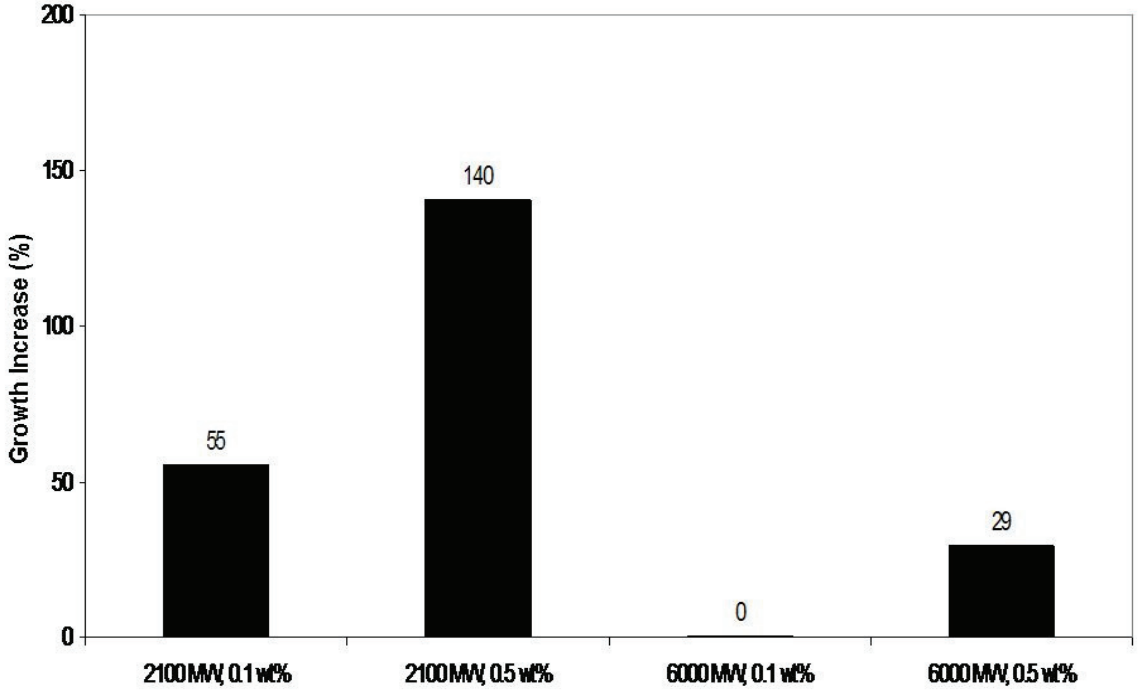

Figure 3.4.7– Growth increaes after 15 minute experimental run for Poly(2- acrylamido-2-methylpropane sulfonic acid), sodium salt at approximately 277.15 K

Table 3.4.2– Experimental Conditions and percentage increase of growth due to promotion % after 6 minutes of experimental run for PAA

#	Solution Name	Conc. (wt%)	MW (g/mole)	Avg. Temp (K)	Avg. Press (kPa)	# of Replicates	Growth Inc. (%)	Moles	Moles Abs. Avg. Dev.
1	Deionized Water	N/A	18	276.95	6498	3	N/A	0.0100	2.66E-04
2	PAA	0.1	2100	277.05	6514	3	55	0.0156	4.29E-04
3	PAA	0.5	2100	277.15	6501	3	140	0.0242	1.01E-03
4	PAA	0.1	6000	277.05	6499	3	0	0.0100	3.11E-04
5	PAA	0.5	6000	277.15	6502	3	23	0.0130	7.58E-05

4 CONCLUSIONS

Experiments were conducted to examine how well Type-I Antifreeze Proteins prevent methane hydrate growth in bulk conditions. Previously, hydrate experiments with AFPs were only done on a small scale, single crystals, less than 10 ml volumes, and with tetrahydrofuran hydrates which are not naturally occurring. This work was done on a larger scale, 250 ml of the solution and with methane hydrates. Results were compared to a commercially made co-polymer kinetic hydrate inhibitor, poly(VP/VC).

In the presence of kinetic inhibitors, hydrate growth curves followed a second order behavior instead of the linear growth trends observed in experiments using deionized water alone. The experimental results suggested that at 277.15 K and 6500 kPa, AFPs inhibit hydrate growth to the same extent as to poly(VP/VC) at the same weight concentration. It was also observed that increasing the concentration of poly(VP/VC) by a factor of 14 improved the inhibition performance by 41%. The effect of temperature and pressure on hydrate growth for poly(VP/VC) and AFP was illustrated. The results show that AFPs inhibit hydrate growth more effectively at a lower hydrate formation driving force. Furthermore, it would appear that AFPs may act as a hydrate growth promoter at 277.15 K and 7200 kPa.

Two polymers poly(2-acrylamido-2-methylpropane sulfonic acid), sodium salt and poly(acrylic acid), sodium salt were tested for hydrate growth for the first time. Both of the two polymers promoted hydrate growth. For poly(2-acrylamido-2-methylpropane sulfonic acid), sodium salt, the hydrate growth was maximum at the highest pressure driving force. For poly(acrylic acid), sodium salt, the hydrate growth was enhanced at lower molecular weights and higher weight concentrations.

5 REFERENCES

Bergeron, S. and Servio, P. (2007) Intrinsic kinetics of propane hydrate formation., *Proceedings of the Eleventh International Conference on Properties and Phase Equilibria for Product and Process Design, Hersonissos*.

Bishnoi,P.R. and Natarajan,V. (1996) Formation and decomposition of gas hydrates. *Fluid Phase Equilibria* **117**, 168-177.

Buffett,B.A. (2000) Clathrate hydrates. *Annual Review of Earth and Planetary Sciences* **28**, 477-507.

Davies,P.L., Baardsnes,J., Kuiper,M.J. and Walker,V.K. (2002) Structure and function of antifreeze proteins. *Philosophical Transactions of the Royal Society of London Series B-Biological Sciences* **357**, 927-933.

DeVries,A.L. and Wohlschl., D.E (1969) Freezing Resistance in Some Antarctic Fishes. *Science* **163**, 1073-&.

Englezos,P., Kalogerakis,N., Dholabhai,P.D. and Bishnoi,P.R. (1987) Kinetics of Formation of Methane and Ethane Gas Hydrates. *Chemical Engineering Science* **42**, 2647-2658.

Englezos,P., Kalogerakis,N., Dholabhai,P.D. and Bishnoi,P.R. (1987) Kinetics of Gas Hydrate Formation from Mixtures of Methane and Ethane. *Chemical Engineering Science* **42**, 2659-2666.

Englezos,P. (1993) Clathrate Hydrates. *Industrial & Engineering Chemistry Research* **32**, 1251-1274.

GPSA handbook vol. II, Ch. 21 Dehydration 1998

Kane, S.G., Evans, T.W. Brian, P.L.T. and Sarofim, A.F. (1974) Determination of the Kinetics of Secondary Nucleation in Batch Crystallizers. *A.I.Ch.E. Journal.* **20**: p. 855-862.

Kelland, M. Thor, S., Øvsthus, J., Tomita, T. and Mizuta, K. (2006) Studies on some alkylamide surfactant gas hydrate anit-agglomerants. *Chemical Engineering Science*, **61**, 4290-4298.

Kim, H.C., Bishnoi, P.R., Heidemann, R.A. and Rizvi, S.S.H. (1987) *Chemical Engineering Science* **42 No.7**, 1645

Koh, C.A., Wescott, R.E., Zhang, W., Hirachand, K., Creek, J.L. and Soper, A.K. (2002) Mechanism of gas hydrate formation and inhibition. *Fluid Phase Equilibria*, **194-197**, 143-151

Kvamme, B., Kuznetsova, T. and Aasolden K. (2005) Molecular dynamics simulation for selection of kinetic hydrate inhibitors. *Journal of Molecular Graphics and Modeling,* **23**, 524-536.

Lederhos,J.P., Long,J.P., Sum,A., Christiansen,R.L. and Sloan,E.D. (1996) Effective kinetic inhibitors for natural gas hydrates. *Chemical Engineering Science* **51**, 1221-1229.

Lee,J.D. and Englezos,P. (2005) Enhancement of the performance of gas hydrate kinetic inhibitors with polyethylene oxide. *Chemical Engineering Science* **60**, 5323-5330.

Lee,J.D. and Englezos,P. (2006) Unusual kinetic inhibitor effects on gas hydrate formation. *Chemical Engineering Science* **61**, 1368-1376.

Matthews,P.N., Subramanian,S. and Creek,J. (2002) High Impact, Poorly Understood Issues with Hydrates In Flow Assurance. *Proceedings of the Forth International Conference on Gas Hydrates*.

Natarjan, V., Bishnoi, P.R. and Kalogerakis, N. (1994) Induction Phenomena in Gas Hydrate Nucleation. *Chemical Engineering Science* **49**, 2075-2087.

Ripmeester,J.A., Tse,J.S., Ratcliffe,C.I. and Powell,B.M. (1987) A New Clathrate Hydrate Structure. *Nature* **325**, 135-136.

Servio,P. and Englezos,P. (2002) Measurement of dissolved methane in water in equilibrium with its hydrate. *Journal of Chemical and Engineering Data* **47**, 87-90.

Sloan Jr,E.D. (1990) Natural Gas Hydrate Phase Equilbria and Kinetics: Understanding the State-of-the-Art, *Rev. Inst. Fr. Pet*., 45 (2), 1990, 245-266.

Sloan Jr, E. D. (1998) Clathrate Hydrates of Natural Gases. New York: Marcel Dekker, Inc.

Suess,E., Bohrmann,G., Greinert,J. and Lausch,E. (1999) Flammable ice. *Scientific American* **281**, 76-83.

Skovborg,P. and Rasmussen,P. (1994) A Mass transport limited Model for the growth of methane and ethane gas hydrates. *Chemical Engineering Science* **49**, 1131-1143.

Trebble,M.A. and Bishnoi,P.R. (1987) Development of A New 4-Parameter Cubic Equation of State. *Fluid Phase Equilibria* **35**, 1-18.

Vysniauskas,A. and Bishnoi,P.R. (1983) A Kinetic-Study of Methane Hydrate Formation. *Chemical Engineering Science* **38**, 1061-1072.

Whiticar, M.J. (2001) Non-Potential of Natural Gas hydrate Occurrence in Queen Charlotte Basin . British Columbia Offshore Hydrocarbon Development **2,** 55-59

Zeng, H. Inhibition of Clathrate Hydrate by Antifreeze Proteins. 2004. Queen's University.
Ref Type: Thesis/Dissertation

Zeng,H., Walker,V.K., Ripmeester,J.A. (2005) Examining the Classification of Low Dosage Hydrate Inhibitors. *Proceedings of the Forth International Conference on Gas Hydrates*.

Zeng,H., Wilson,L.D., Walker,V.K. and Ripmeester,J.A. (2006) Effect of antifreeze proteins on the nucleaton, growth, and the memory effect during tetrahydrofuran clathrate hydrate formation. *Journal of the American Chemical Society* **128**, 2844-2850.

Zhong,Y. and Rogers,R.E. (2000) Surfactant effects on gas hydrate formation. *Chemical Engineering Science* **55**, 4175-4187.

Zongchao,J. and Davies,P.L. (2002) Antifreeze proteins: an unusual receptor-ligand interaction. *TRENDS in Biochemical Sciences* **27**, 101-106.